Journal of Sound and Vibration (1999) **224**(1), 123–165
Article No. jsvi.1999.2169, available online at http://www.idealibrary.com on IDEAL®

AN INTEGRATED MODEL FOR DRILL-STRING DYNAMICS

R. W. TUCKER AND C. WANG
*Department of Physics, Lancaster University, LA*1 4*YB, England*

(*Received* 5 *August* 1998, *and in final form* 3 *February* 1999)

The vibrational states experienced by the active components of a drilling assembly such as that found in the oil or gas industry are discussed in the context of an integrated mathematical model. The work is motivated by the need to understand the complex vibrational states that such a system can exhibit in order to better control their constructive and destructive potential. The model is expressed in terms of six continuous independent degrees of freedom. Three locate the position of the centroid of the drill-string in space and three permit the dynamical state of the drill-string to be expressed in terms of flexural, torsional and shear strain, together with dilation and stretch. By supplementing the model with appropriate constitutive relations that relate these strains to bending and twisting couples together with shear and compression forces it can fully accommodate the modes of vibration that are traditionally associated with the motion of drill-strings in both straight and curved boreholes discussed in the engineering literature. These include axial motion along the length of the drill-string, torsional or rotational motion and transverse or lateral motion. Attention is given to the boundary conditions appropriate for an active drill-string and BHA stabiliser including an account of frictional simulations at the rock-interface, cutter simulations for different types of drill-bit and interactions between the bore cavity and the drill-string. The model is used to discuss the stability of axisymmetric drill-string configurations in vertical boreholes under both coupled torsional, axial and lateral perturbations as well as general non-perturbative coupled vibrational states under extreme conditions of lateral whirl.

1. INTRODUCTION

This article develops a model for the dynamical behaviour of an active drilling assembly as used in the oil or gas industry. It is motivated by the need to understand the complex vibrational states experienced by such a system in order to better control their constructive and destructive potential. A drilling assembly consists essentially of a series of hollow cylindrical steel pipes connected to form a long flexible *drill-string* to which is attached a short heavier segment containing a cutting device at the free end (the *drill bit*). This segment may contain stabilising fins designed to minimise lateral motion during drilling and together with the drill-bit constitutes the *bottom-hole assembly* (BHA). The drill-string is

0022–460X/99/260123 + 43 $30.00/0

driven in a rotary fashion from the top end, often by means of an electric motor and gearbox, the *top-drive*, and constrained to pass at a controlled rate through a rotating mass (the *rotary*) near the surface. Such a drilling system is designed to construct a borehole linking the earth's surface to a reservoir of oil or gas. The borehole is lined (usually with steel) and the excess in the diameter of this cavity over the diameter of the drill-pipe is referred to below as the *overgauge*. This annular gap (which in general varies along the bore-hole) is necessary for the conduction of fluids. These are a source of external interaction along the drill-string in addition to gravity and the bore-liner. During the process of drilling, pressurised fluid (*mud*) is continuously circulated down the centre of the drill-string, out of holes in the drill-bit and back to the surface via the space between the rotating drill-string and the surface of the bore-hole. Its primary purpose is to cool and lubricate the drill-bit as well as to remove cuttings produced by the bit. Such a system is prone to dynamic instabilities that are not fully understood. Field experience provides ample testament to the destructive consequences of such instabilities.

Although there exists an extensive literature devoted to the analysis of distinct aspects of the dynamics of the drill-string and BHA [1–3] it is only recently that the virtues of treating the drilling assembly as an integrated system have been considered. Since the physics involved is inherently non-linear and recourse to modelling is inevitable to compensate for a lack of detailed dynamical information in the vicinity of the bit, many conclusions have been based on numerical simulations that ignore one or more aspects of the problem. In the authors' view the lack of a coherent model in the literature that is free from unwarranted assumptions makes it difficult to accurately assess the nature of many approximate treatments and thereby to get a clear overview of the significance of model predictions. The approach here is to formulate a mathematically well defined dynamical model that permits control of the approximations involved, is not computationally over-expensive and has the potential to accommodate the many complexities of a realistic drilling assembly and its environment.

The motion of the drill-string may be described in terms of the motion in space of the line of centroids of its cross-sections and its elastic deformations about that line. The steel strings under consideration have a ratio of average diameter to length of order 10^{-5} (which is less than that of the average human hair). Due to the earth's gravity their horizontal length differs from their vertical length by between 1 and 2 m. This suggests that they can be effectively modelled by elastic space-curves with structure. This structure defines the relative orientation of neighbouring cross-sections along the drill-string. Specifying a unit vector (which may be identified with the normal to the cross-section) at each point along the drill-string centroid enables the state of flexure to be related to the angle between this vector and the tangent to the space-curve (Figure 1). Specifying a second vector orthogonal to the first vector (thereby placing it in the plane of the cross-section) can be used to encode the state of bending and twist along the drill-string. Thus a field of two mutually orthogonal unit vectors along the drill-string provides three continuous dynamical degrees of freedom

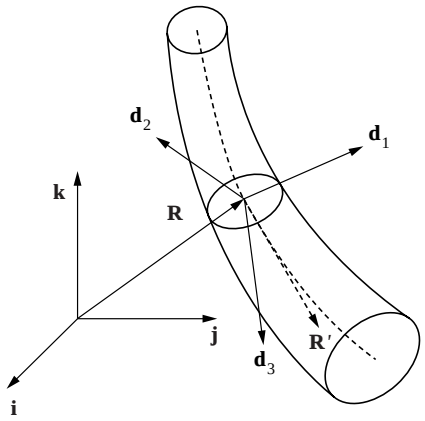

Figure 1. The motion of a drill-string segment may be described in terms of the motion in space of a vector **R** that locates the line of centroids (shown dotted) of the cross-sections of the drill-string. Specifying a unit vector $\mathbf{d}_3$ (which may be identified with the normal to the cross-section) at each point along this line enables the state of flexure to be related to the angle between this vector and the tangent $\mathbf{R}'$ to the centroid space-curve. Specifying a second vector $\mathbf{d}_2$ orthogonal to the first vector (thereby placing it in the plane of the cross-section) can be used to encode the state of bending and twist along the drill-string. Elastic deformations about the line of centroids are then coded into the rates of change of **R** and the triad $\{\mathbf{d}_1, \mathbf{d}_2, \mathbf{d}_3 = \mathbf{d}_1 \times \mathbf{d}_2\}$ along the drill-string. Thus a time dependent field of two mutually orthogonal unit vectors along the drill-string provides three continuous dynamical degrees of freedom that, together with the three continuous degrees of freedom describing the centroid space-curve relative to some arbitrary origin in space (with fixed inertial frame $\{\mathbf{i}, \mathbf{j}, \mathbf{k}\}$), define a simple Cosserat rod model.

that, together with the continuous three degrees of freedom describing a space-curve relative to some arbitrary origin in space, define a simple Cosserat rod model. The dynamical equations of motion for these continuous six degrees of freedom are presented in section 2 and this is the model adopted here for a drill-string. Supplemented with appropriate constitutive relations and boundary conditions it can fully accommodate the modes of vibration that are traditionally associated with the motion of drill-strings in the engineering literature: namely axial motion along the length of the drill-string, torsional or rotational motion and transverse or lateral motion. These modes will be clearly defined in terms of the model adopted here.

Although the model accommodates arbitrary displacements and deformations its linearisations about various stationary configurations offer valuable guidance for the attainment of stable drilling processes. The fully non-linear aspects of the motion are however needed to appreciate the significance of some of the most important non-perturbative vibrational phenomena observed in the field [4, 5]. These include torsional relaxation oscillations induced by non-linear frictional torques between the drill-bit at the rock surface (*torsional "slip–stick"*), axial vibrations that induce the drill-bit to intermittently lose contact with the rock surface (*"bit-bounce"*), whirling motion of the drill-string and the motion of the bit in the borehole (bit and BHA-whirl).

Torsional "slip–stick" is often regarded as one of the most damaging modes of vibration when drilling with low rotary speeds [6]. For a typical drill-string of length around 5000 m such a torsional disturbance consists of a travelling

torsional pulse that bounces back and forth between the top rotary and the drill-bit every few seconds periodically forcing the drill-bit to ''slip'' and ''stick'' for extended periods at the rock surface. The amplitude of this torsional excitation can be two to four times the target or average angular speed (typically between 30 and 150 r.p.m.) set by the top-drive and this can give rise to enormously destructive fluctuating torques in the drill-string that, once out of control, invariably cause damage to the bit or drill-string. Even small amplitude ''slip–stick'' vibrations are thought to be a major cause of bit wear. Various control techniques have been devised to combat this instability [7–11] but field evidence [12, 13] suggests that they often exhibit undesirable volatility thereby detracting from their overall efficiency. In section 13 this feature is mentioned in the context of the model under discussion and an alternative suggested.

In addition to these violent excitations that can lead to rapid failure in the drilling operation there are more subtle vibrations that are thought to contribute to fatigue crack growth leading to ultimate failure of components. These include the transfer of energy between axial [14], lateral and torsional motion [15] induced by the interactions of the drill-string and BHA with their environment. The nature of such inter-mode coupling can be dramatically influenced by drilling strategies and initial conditions. Such interrelated phenomena demand a fully integrated model capable of assessing the significance of the boundary conditions in the evolution of the model. The model formulated here offers such an integrated description of the drilling process and provides boundary and initial conditions for a solution to the ensuing quasilinear hyperbolic system of partial differential equations in two independent variables.

In section 2 the mathematical formulation of the model is presented together with appropriate junction and boundary conditions. This section also discusses the constitutive equations needed to complete the equations of motion of the drill-string. In the remaining sections particular solutions are discussed. These include static solutions and the notion of ''weight on bit'', stability analyses, non-perturbative torsional and axial vibrations and whirling solutions. In the axially symmetric sector a discussion of linearisation stability is given and the exact equations of motion are reduced to the solution of a system of ordinary differential–difference equations. This provides a valuable approach to a numerical simulation that is free from spatial discretisation and is thereby ideally suited to study vibrational phenomena to higher frequencies than is possible with traditional finite element techniques. Finally the restriction to axial symmetry is released and a full simulation explored using a new numerical approach based on a semi-implicit method applied to a system of stiff ordinary differential equations.

2. EQUATIONS OF MOTION

The general mathematical theory of non-linear elasticity is well established. The general theory of one-dimensional Cosserat continua derived as limits of three-dimensional continua can be consulted in Antman [16]. The theory is fundamentally formulated in the Lagrangian picture in which material elements

of a rod labelled by s. The dynamical evolution of the drill-string with mass density, $s \in [0, L_0] \mapsto \rho(s)$, and cross-sectional area, $s \in \mapsto A(s)$, is governed by Newton's dynamical laws:

$$\rho A \ddot{\mathbf{R}} = \mathbf{n}' + \mathbf{f}, \quad \partial_t(\rho \mathbf{I}(\mathbf{w})) = \mathbf{m}' + \mathbf{R}' \cdot \mathbf{n} + \mathbf{l} \tag{1, 2}$$

applied to a triad of orthonormal vectors:

$$s \in [0, L_0] \mapsto \{\mathbf{d}_1(s, t), \mathbf{d}_2(s, t), \mathbf{d}_3(s, t)\} \tag{3}$$

over the space-curve:

$$s \in [0, L_0] \mapsto \mathbf{R}(s, t), \tag{4}$$

at time t where $\mathbf{n}' = \partial_s \mathbf{n}$, $\dot{\mathbf{R}} = \partial_t \mathbf{R}$, $\mathbf{f}$ and $\mathbf{l}$ denote external force and torque densities respectively and $s \in [0, L_0] \mapsto \mathbf{I} \mapsto \rho \mathbf{I}$ is a drill-string moment of inertia tensor. In these field equations the contact *forces* $\mathbf{n}$ and contact *torques* $\mathbf{m}$ are related to the *strains* $\mathbf{u}$, $\mathbf{v}$, $\mathbf{w}$ by constitutive relations. The strains are themselves defined in terms of the configuration variables $\mathbf{R}$ and $\mathbf{d}_k$ for $k = 1, 2, 3$ by the relations:

$$\mathbf{R}' = \mathbf{v}, \quad \mathbf{d}_k' = \mathbf{u} \times \mathbf{d}_k, \quad \dot{\mathbf{d}}_k = \mathbf{w} \times \mathbf{d}_k. \tag{5–7}$$

The latter ensures that the triad remains orthonormal under evolution. The last equation identifies

$$\mathbf{w} = \tfrac{1}{2} \sum_{k=1}^{3} \mathbf{d}_k \times \dot{\mathbf{d}}_k, \tag{8}$$

with the local angular velocity vector of the director triad.

The general model accommodates continua whose characteristics (density, cross-sectional area, rotary inertia) vary with s. For a system in which the elastodynamics of the BHA are significant one considers two coupled continua with different elastic characteristics described by equations (1), (2) on $0 \leqslant s < s_0$ and $s_0 < s \leqslant L_0$ respectively, each subject to their associated constitutive relations. One then matches the degrees of freedom at $s = s_0$ according to a junction condition describing the manner in which the drill-string is connected to the BHA. For certain couplings (e.g., Oldham's joint [17]) the evaluation of constraint forces and torques becomes important. If the characteristics change discontinuously at some point (e.g., where the drill-bit interacts with the rock base or drill-strings with different characteristics are joined together or with the BHA) conditions on the contact forces and torques on either side, $\pm$, of the junction must be satisfied. If a rigid body of mass M_0 and rotary inertia tensor I_0 is also attached to the point then discontinuous contact forces and torques contribute to the equations of motion of such an attachment. In general for such a junction at $s = s_0$, the contact forces and couples are subject to the discontinuity conditions:

$$\mathbf{n}^+(s_0, t) - \mathbf{n}^-(s_0, t) + \mathbf{F}_0(s_0, t) = M_0 \ddot{\mathbf{R}}(s_0, t) \tag{9}$$

and

$$\mathbf{m}^{+}(s_0, t) - \mathbf{m}^{-}(s_0, t) + \mathbf{G}_0(s_0, t) = I_0(\dot{\mathbf{w}}(s_0, t)). \tag{10}$$

In these equations $\mathbf{F}_0(s_0, t)$ and $\mathbf{G}_0(s_0, t)$ denote the external forces and torques acting at $s = s_0$.

In view of the comments above about the relative spatial dimensions of drill-strings in deep wells, in this article the BHA and rotary will be treated as mass points with rotary inertia attached to the ends of the drill-string. The effects of the BHA stabilisers will be modelled by boundary conditions (discussed below) which constrain the direction of the tangent to the drill-string at the drill-bit.

To close the above equations of motion constitutive relations appropriate to the active drill-string must be specified:

$$\mathbf{n}(s, t) = \hat{\mathbf{n}}(\mathbf{u}(s, t), \mathbf{v}(s, t), \mathbf{u}_t(s, t), \mathbf{v}_t(s, t), \ldots, s), \tag{11}$$

$$\mathbf{m}(s, t) = \hat{\mathbf{m}}(\mathbf{u}(s, t), \mathbf{v}(s, t), \mathbf{u}_t(s, t), \mathbf{v}_t(s, t), \ldots, s). \tag{12}$$

These relations specify a "natural" reference configuration (say $t = 0$) with strains $\mathbf{U}(s)$, $\mathbf{V}(s)$ such that

$$\hat{\mathbf{n}}(\mathbf{U}(s), \mathbf{V}(s), \ldots, s) = 0, \quad \hat{\mathbf{m}}(\mathbf{U}(s), \mathbf{V}(s), \ldots, s) = 0. \tag{13, 14}$$

A standard reference configuration has $\mathbf{R}'_s(s, 0) = \mathbf{d}_3(s, 0)$, i.e.,

$$\mathbf{V}(s) = \mathbf{d}_3(s, 0). \tag{15}$$

If this standard configuration is such that $\mathbf{R}(s, 0)$ is a space-curve with Frenet curvature κ_0 and torsion τ_0 and the standard directors are oriented so that $\mathbf{d}_1(s, 0)$ is the unit normal to the space-curve and $\mathbf{d}_2(s, 0)$ the associated unit binormal then

$$\mathbf{U}(s) = \kappa_0(s)\mathbf{d}_2(s, 0) + \tau_0(s)\mathbf{d}_3(s, 0). \tag{16}$$

This follows immediately from the definition (6) of $\mathbf{u}$ and the Frenet–Serret equations [18] for the space-curve:

$$\mathbf{d}'_3(s, 0) = \kappa_0(s)\mathbf{d}_1(s, 0), \quad \mathbf{d}'_1(s, 0) = -\kappa_0(s)\mathbf{d}_3(s, 0) + \tau_0(s)\mathbf{d}_2(s, 0), \tag{17, 18}$$

$$\mathbf{d}'_2(s, 0) = -\tau_0(s)\mathbf{d}_1(s, 0). \tag{19}$$

The use of a curved standard configuration has immediate application to the dynamics of drill-strings in curved bore-holes. These are used in long-reach operations where under-sea exploration is initiated from land-based drilling rigs. In some cases an initially vertical drill-string is guided into a horizontal configuration under the sea-bed for several kilometres. In this article attention is restricted to vertical straight bore-holes and a space-curve with zero curvature and torsion defines the natural unstressed configuration of the drill-string. Thus the reference state of the drill-string in the absence of gravity is $\{\mathbf{R}(s, t) = -s\mathbf{k}, \mathbf{d}_1(s, t) = \mathbf{i}, \mathbf{d}_2(s, t) = -\mathbf{j}, \mathbf{d}_3(s, t) = -\mathbf{k}\}$ where $s \in [0, L_0]$. The value of L_0 is the physical length of the unstressed drill-string in the absence of gravity.

The simplest constitutive model to consider is based on Kirchoff constitutive relations with shear deformation. Such a model exhibits a rich dynamical behaviour that accommodates all the phenomena alluded to in the introduction. The presence of arbitrary rotations relating the local director frame to the global inertial frame renders the equations of motion inherently non-linear. One may exploit the full versatility of the Cosserat model by generalising the Kirchoff constitutive relations to include viscoelasticity and other damping, curved reference states with memory and effects to prohibit total compression. Such generalisations will be mentioned although not pursued in detail in this article.

As a prelude to casting all equations into dimensionless form it is useful to introduce some natural scales that facilitate this exercise. For a drill-string with Young's modulus of elasticity E and shear modulus G with (dimensions $[ML^{-1}T^{-2}]$) a natural unit of time is chosen to be $T_0 = L_0/c$ where $c^2 = E/\rho$. This suggests the introduction of the dimensionless evolution parameter $\eta = t/T_0$. Similarly defining $\sigma = s/L_0$, where $0 \leqslant s \leqslant L_0$, implies $0 \leqslant \sigma \leqslant 1$.

Besides the global orthonormal Cartesian frame $\{\mathbf{i}, \mathbf{j}, \mathbf{k}\}$ the directors $\{\mathbf{d}_1, \mathbf{d}_2, \mathbf{d}_3 = \mathbf{d}_1 \times \mathbf{d}_2\}$, provide a local dimensionless oriented orthonormal director frame $\{\mathbf{d}_k\}$ (with dual basis $\widetilde{\mathbf{d}^{(k)}}$) in which to define the components of the drill-string rotary inertia tensor per unit reference length, $(\rho\mathbf{I})$, (with dimensions $[ML]$):

$$\begin{aligned}(\rho\mathbf{I})(s,t) = {} & I_{1,1}(s,t)(\widetilde{\mathbf{d}_1(s,t)}) \otimes \mathbf{d}_1(s,t) + I_{2,2}(s,t)(\widetilde{\mathbf{d}_2(s,t)}) \otimes \mathbf{d}_2(s,t) \\ & + I_{3,3}(s,t)(\widetilde{\mathbf{d}_3(s,t)}) \otimes \mathbf{d}_3(s,t) + I_{1,2}(s,t)(\widetilde{\mathbf{d}_1(s,t)}) \otimes \mathbf{d}_2(s,t) \\ & + I_{2,1}(s,t)(\widetilde{\mathbf{d}_2(s,t)}) \otimes \mathbf{d}_1(s,t), \end{aligned} \tag{20}$$

where the components are given as integrals over the cross-sectional area $A(s)$:

$$I_{1,1}(s,t) = \int_{A(s)} \rho y^2 \, \mathrm{d}x \wedge \mathrm{d}y, \quad I_{2,2}(s,t) = \int_{A(s)} \rho x^2 \, \mathrm{d}x \wedge \mathrm{d}y, \tag{21, 22}$$

$$I_{3,3}(s,t) = \int_{A(s)} \rho(x^2 + y^2) \, \mathrm{d}x \wedge \mathrm{d}y, \tag{23}$$

$$I_{1,2}(s,t) = I_{2,1}(s,t) = -\int_{A(s)} \rho xy \, \mathrm{d}x \wedge \mathrm{d}y. \tag{24}$$

It will be assumed that the drill-string is a right-cylindrical shell and composed of material with a uniform mass density $\rho = \rho_0$ having an annular cross-section of outer radius r_0 and inner radius r_i. Then

$$I_{1,1} = I_{2,2} = \pi\rho_0(r_o^4 - r_i^4)/4, \quad I_{3,3} = \pi\rho_0(r_o^4 - r_i^4)/2, \quad I_{1,2} = 0. \tag{25–27}$$

In terms of the drill-string area moments $K_{11} = I_{11}/\rho_0$ and $K_{22} = I_{22}/\rho_0$ (with dimensions $[L^4]$) the torsional rigidity of the drill-string is $\mathcal{D} = G(K_{11} + K_{22})$. These considerations suggest the introduction of a natural torque unit $\mathcal{G} = GK_{\alpha\alpha}/L_0$ with dimensions $[ML^2T^{-2}]$ and transverse area moment $K_{\alpha\alpha} = (K_{11} + K_{22})$

together with a natural force unit EA with dimensions $[MLT^{-2}]$. All quantities will henceforth be scaled into dimensionless form using these natural scales. A conversion table is given in Appendix 1 which also contains numerical data used in subsequent simulations.

The dynamical equations of motion for the drill-string are now given in dimensionless form as

$$\mathbf{R}_{\eta\eta} = \mathbf{n}_\sigma - g\mathbf{k} + \mathbf{f}, \quad ((\rho\mathbf{I})(\mathbf{w}))_\eta = \mathbf{m}_\sigma + \kappa(\mathbf{R}_\sigma \times \mathbf{n}) + \mathbf{l}, \tag{28, 29}$$

$$\partial_\sigma \mathbf{d}_k = \mathbf{u} \times \mathbf{d}_k, \quad \partial_\eta \mathbf{d}_k = \mathbf{w} \times \mathbf{d}_k, \quad \mathbf{R}_\sigma = \mathbf{v}, \tag{30–32}$$

where $\kappa = EAL_0/\mathcal{G}$ for a drill-string with cross-sectional area A.

With

$$\mathbf{n} = n_1\mathbf{d}_1 + n_2\mathbf{d}_2 + n_3\mathbf{d}_3, \quad \mathbf{m} = m_1\mathbf{d}_1 + m_2\mathbf{d}_2 + m_3\mathbf{d}_3, \tag{33, 34}$$

$$\mathbf{v} = v_1\mathbf{d}_1 + v_2\mathbf{d}_2 + v_3\mathbf{d}_3, \quad \mathbf{u} = u_1\mathbf{d}_1 + u_2\mathbf{d}_2 + u_3\mathbf{d}_3, \quad \mathbf{w} = w_1\mathbf{d}_1 + w_2\mathbf{d}_2 + w_3\mathbf{d}_3, \tag{35–37}$$

the classical Kirchoff constitutive relations may be written in dimensionless form as:

$$n_1 = \chi v_1, \quad n_2 = \chi v_2, \quad n_3 = v_2 - 1, \tag{38–40}$$

$$m_1 = I_{11}u_1 + I_{12}u_2, \quad m_2 = I_{12}u_1 + I_{22}u_2, \quad m_3 = u_3, \tag{41–43}$$

where the dimensionless parameter $\chi = G/E$.

The generalisation of these relations to include viscoelasticity and a curved drill-string requires the introduction of the dimensionless positive viscoelasticity parameters $\{\alpha_{n1}, \alpha_{n2}, \alpha_{n3}, \alpha_{m1}, \alpha_{m2}, \alpha_{m3}\}$ and the functions $\{\sigma \mapsto U_2(\sigma), \sigma \mapsto U_3(\sigma)\}$ defining the curvature and torsion of the reference space-curve:

$$n_1 = \chi(v_1 + \alpha_{n1}v_{1\eta}), \quad n_2 = \chi(v_2 + \alpha_{n2}v_{2\eta}), \quad n_3 = (v_3 + \alpha_{n3}v_{3\eta}) - 1, \tag{44–46}$$

$$m_1 = I_{11}(u_1 + \alpha_{m1}u_{1\eta}) + I_{12}(u_2 - U_2 + \alpha_{m2}u_{2\eta}), \tag{47}$$

$$m_2 = I_{12}(u_1 + \alpha_{m1}u_{1\eta}) + I_{22}(u_2 - U_2 + \alpha_{m2}u_{2\eta}), \tag{48}$$

$$m_3 = (u_3 - U_3 + \alpha_{m3}u_{3\eta}). \tag{49}$$

The Kirchoff constitutive relations permit one to identify: flexural strains $\equiv \{u_1, u_2\}$; torsional strain $\equiv \{u_3\}$; shear strains $\equiv \{v_1, v_2\}$; dilation strain $\equiv \{v_3\}$; stretch $\equiv |\mathbf{v}|$, and relate them to: bending couples $\{m_1, m_2\}$; twisting couple $\{m_3\}$; shear forces $\{n_1, n_2\}$, tension or compression $\{n_3\}$ if $\mathbf{v} \times \mathbf{n} = 0$.

3. STATIC CONFIGURATIONS

A basic configuration corresponds to a static (non-rotating) vertical drill-string with the drill-bit either suspended in an empty bore-hole or in contact with the rock surface at its base. If in contact the bit-reaction force on the drill-bit is determined by the drilling engineer who controls the tension (or compression) in the cable that is used to connect the drill-string to the drilling rig fixed at the surface. This bit-reaction force is known as the (*static*) "weight-on-bit" and is clearly the difference between the weight of the complete drilling assembly and the vertical force in the top cable. Varying this force whilst drilling is one of the primary mechanisms that controls the drilling process. Since the initial "weight-on-bit" is a valuable parameter in describing the initial conditions it is worthwhile to make precise a class of static solutions to equations (28–43). In terms of the global inertial frame $\{\mathbf{i}, \mathbf{j}, \mathbf{k}\}$ with $\mathbf{k} = \mathbf{i} \times \mathbf{j}$ vertical and origin at the rotary, these solutions take the form:

$$\mathbf{R} = Z(\sigma)\mathbf{k}, \quad \{\mathbf{d}_1(\sigma, \eta) = \mathbf{i}, \mathbf{d}_2(\sigma, \eta) = -\mathbf{j}, \mathbf{d}_3(\sigma, \eta) = -\mathbf{k}\}, \tag{50, 51}$$

with $\mathbf{v}(\sigma, \eta) = Z_\sigma(\sigma)\mathbf{K}$ and hence $\mathbf{n}(\sigma, \eta) = (Z_\sigma(\sigma) + 1)\mathbf{k}$. In terms of the effective scaled masses of the top-drive and BHA, μ_{top} and μ_{bit} the solutions to the non-trivial static equations

$$\mathbf{n}(0, \eta) - \mu_{top} g\mathbf{k} + \mathbf{F}^{top}(\eta) = 0, \mathbf{n}_\sigma(\sigma, \eta) - g\mathbf{k} = 0, \ -\mathbf{n}(1, \eta) - \mu_{bit} g\mathbf{k} + \mathbf{F}^{bit}(\eta) = 0, \tag{52–54}$$

can be written

$$Z(\sigma) - Z(0) = g\sigma^2/2 + (g\mu_{top} - 1 - f^{top})\sigma, \tag{55}$$

or equivalently

$$Z(\sigma) - Z(1) = g(\sigma^2 - 1)/2 + (f^{bit} - g\mu_{bit} - 1)(\sigma - 1), \tag{56}$$

where $\mathbf{F}^{top}(\eta) = f^{top}\mathbf{k}$, $\mathbf{F}^{bit}(\eta) = f^{bit}\mathbf{k}$ and

$$f^{bit} + f^{top} = g(1 + \mu_{bit} + \mu_{top}). \tag{57}$$

f^{bit} is the magnitude of the *static* "weight-on-bit".* If the top force $f^{top} > 0$ then f^{bit} is less than the total weight $g(1 + \mu_{bit} + \mu_{top})$ of the drill-string, drill-bit and rotary and the top cable is in tension. If $f^{top} < 0$ then f^{bit} exceeds the total weight and the top force is compressive. If $f^{bit} = 0$ then the force in the top cable just supports the total weight implying a loss of contact of the drill-bit with the rock surface. This will be referred to as a static hanging configuration.

It is convenient to label solutions by δZ where $Z(1) = -1 - \delta Z$. Then it follows that

$$f^{bit} = \mu_{bit} g + g/2 - \delta Z, \quad f^{top} = \mu_{top} g + g/2 + \delta Z, \tag{58, 59}$$

*If the environment of the drill-string contains static fluid then the weight of the drill-string is reduced by the buoyancy provided by the displaced fluid.

and the drill-string exceeds its reference length if $\delta Z > 0$, is hanging vertically from the top cable if $f^{bit} = 0$ with $\delta Z = (2\mu_{bit} + 1)g/2$ and is compressed if $\delta Z < 0$. The state of stress in the static drill-string may change from tension to compression if the neutral point $\sigma = \sigma_0 \equiv 1/2 + \delta Z/g$ given by $\mathbf{n}(\sigma_0, \eta) = 0$ lies in the range $0 \leqslant \sigma_0 \leqslant 1$. Thus a static configuration of a vertical drill-string may be specified by δZ. The constitutive relation (40) is designed for $|\delta Z| \ll 1$ otherwise it would need modification to prevent total compression or the inclusion of plasticity. Such modifications are not relevant for drill-string systems.

4. BOUNDARY CONDITIONS

One assumes that the drill-string is connected to effective masses μ_{top} and μ_{bit} modelling the top drive and BHA respectively, and point rigid bodies with rotary inertia tensors $\mathbf{J}^{top}$ and $\mathbf{J}^{bit}$ modelling the rotary and drill-bit respectively. The top-drive connection to the drill-string is located at $\sigma = 0$ and the drill-bit is located at $\sigma = 1$. At these points, forces $\mathbf{F}^{top}(\eta)$ and $\mathbf{F}^{bit}(\eta)$ and torques $\mathbf{L}^{top}(\eta)$ act. The nature of these forces depends on the way the boundary conditions are implemented. In some circumstances certain of their components may be prescribed (e.g., by the frictional forces or drive torques in evidence) while other components may be determined dynamically by the constraints in evidence (e.g., the way the stabilisers interact with the borehole in the BHA). The basic boundary conditions that follow from the discontinuity relations (9), (10) are then:

$$\mu_{top}\mathbf{R}(0, \eta)_{\eta\eta} = \mathbf{n}(0, \eta) - \mu_{top}g\mathbf{k} + \mathbf{F}^{top}(\eta), \tag{60}$$

$$(\mathbf{J}^{top}(\mathbf{w}))_{\eta}(0, \eta) = \mathbf{m}(0, \eta) + \mathbf{L}^{top}(\eta), \tag{61}$$

at $\sigma = 0$ and

$$\mu_{bit}\mathbf{R}(1, \eta)_{\eta\eta} = -\mathbf{n}(1, \eta) - \mu_{bit}g\mathbf{k} + \mathbf{F}^{bit}(\eta), \tag{62}$$

$$(\mathbf{J}^{bit}(\mathbf{w}))_{\eta}(1, \eta) = -\mathbf{m}(1, \eta) + \mathbf{L}^{bit}(\eta), \tag{63}$$

at $\sigma = 1$. The implementation of these boundary conditions can be a matter of some expediency in order to match the model as closely as possible with the way in which an actual drilling process is executed. This is because the process is essentially controlled by varying the magnitude of the tension in the cable attached to the drill-string at the top, the voltage and current in the electric motor that delivers the torque to the drill-string and the manner in which the drill-string itself is lowered through the rotary to accommodate the penetration of the bit into the rock. If the motion of the latter is prescribed so that

$$\mathbf{R}(0, \eta) = \Lambda^{\mathrm{T}}(\eta)\mathbf{k}, \tag{64}$$

then the top constraining force is determined from:

$$\mathbf{F}^{top}(\eta) = \mu_{top}\mathbf{R}(0, \eta)_{\eta\eta} - \mathbf{n}(0, \eta) + \mu_{top}g\mathbf{k}, \tag{65}$$

in terms of the contact force $\mathbf{n}(0, \eta)$. The electric motor is designed to deliver torque that drives the entire drill-string towards a uniform (target) angular speed Ω_0. It also responds to signals from various control feedback devices that are designed to expedite a smooth as possible evolution towards this target state. If one assumes that the rotary is rotationally unconstrained and that the transmission of the torque to the rotary is similarly unconstrained then the torque boundary condition to be satisfied at $\sigma = 0$ is

$$(\mathbf{J}^{top}(\mathbf{w}))_{\eta}(0, \eta) = \mathbf{m}(0, \eta) + \mathbf{L}^{top}(\eta). \tag{66}$$

In this equation the control torque takes the form:

$$\mathbf{L}^{top}(\eta) = T_M(\eta)\mathbf{d}^{(3)}(0, \eta) + \lambda\mathbf{\Psi}(\eta). \tag{67}$$

The standard control torque provided by the drive motor is

$$T_M(\eta) = \kappa_i\xi(\eta) + \kappa_p\xi_{\eta}(\eta), \tag{68}$$

where

$$\xi_{\eta}(\eta) = \Omega_0 + w_3(0, \eta) - hT_f(\eta), \tag{69}$$

and h, κ_i, κ_p are positive control parameters. The most primitive system is an angular speed-controller with $h = 0$, $\lambda = 0$ and target speed $|\Omega_0|$. In so called "soft-torque" control systems $h \neq 0$, $\lambda = 0$ and $T_f(\eta)$ is derived from the output $T_c(\eta)$ of some AC low-pass filter applied to the contact torque at (or near) the rotary*:

$$T_f(\eta) = -m_3(0, \eta) - T_c(\eta). \tag{70}$$

In reference [19] an alternative to conventional "soft-torque" control has been proposed based on the rectification of travelling torsional waves on the drill-string and its effectiveness in model simulations. This additional control with $\lambda > 0$ is defined by

$$\mathbf{\Psi}(\eta) = \mathbf{w}(0, \eta) - \gamma\mathbf{m}(0, \eta) \tag{71}$$

in the control torque above. The constant γ depends on the speed of travelling torsional waves and the torsional rigidity of the drill-string [19]. In the simulations discussed in this article attention is restricted to the simplest speed-controller with $h = 0$, $\lambda = 0$.

In practice the rotary is constrained by bearings to rotate in a fixed horizontal plane. In vertical drilling this is orthogonal to the tangent to the drill-string as it passes through the rotary. In these circumstances $\mathbf{d}_3(0, \eta)$ is replaced by $\pm\mathbf{k}$ in the control torque above and only the $\mathbf{k}$ component of (66) is imposed. The constraint on the rotary can be modelled by $\mathbf{R}_{\sigma}(0, \eta)\cdot\mathbf{i} = 0$, $\mathbf{R}_{\sigma}(0, \eta)\cdot\mathbf{j} = 0$.

*In the simplest case $T_{c\eta}(\eta) = -\omega_c(m_3(0, \eta) + T_c(\eta))$ for some cut-off angular frequency ω_c.

These constraints imply the existence of constraining torques in $\mathbf{L}^{top}(\eta)$ in the $\mathbf{i}$ and $\mathbf{j}$ directions which may be determined from the projection of (66) in these directions.

The implementation of the boundary conditions at $\sigma = 1$ is more involved. In addition to possible constraining torques on the BHA induced by the stabilisers one has to take into account the effects of friction and forces induced by the drill-bit in interaction with the rock surface. Furthermore as a result of cutting activity the rock surface is itself mobile. The friction at the drill-bit may be classified into Coulombic and viscous type. The former is usually regarded as dominant in drilling dynamics. Its characteristic feature is the variation with relative motion which in general is restricted to a domain about zero where it depends on the ambient forces [19–23]. In the following this behaviour will be modelled on field data. The Coulombic component of sliding and torque friction will be parametrised by real valued functions of relative motion, μ and $\mathcal{F}$ respectively. The dynamics of the cutting process itself will be encoded into a dynamical rock surface (parametrised by amplitudes $r_{l,m}(\eta)$) representing the manner in which the drill-bit removes cuttings from this surface. The shape of the surface is determined by these amplitudes and a dynamic function $\Lambda^B(\eta)$ that describes the penetration of the drill-bit into the rock formation. The bore-hole is defined to be a right-cylinder of radius R_b and length $\Lambda^B(\eta)$ capped at the bottom with the dynamic surface $\Sigma(\eta)$.

With respect to a fixed origin in space at the centre of the upper end of this cylinder the surface $\Sigma(\eta)$ is described by the vector

$$\mathbf{r}(\theta, \phi, \eta) = (\Lambda^B(\eta) + \sqrt{R_f^2 - R_b^2})\mathbf{k} + r_f(\theta, \phi, \eta)\{\sin\theta\cos\phi\mathbf{i} + \sin\theta\sin\phi\mathbf{j} + \cos\theta\mathbf{k}\}, \tag{72}$$

where

$$r_f(\theta, \phi, \eta) = R_f + \sum_l \sum_{m=-l}^{m=1} r_{lm}(\eta)\{\mathrm{Y}_l^m(\theta, \phi) - \mathrm{Y}_l^m(\alpha, \phi)\} \tag{73}$$

for some prescribed function $\Lambda^B(\eta)$, $r_{lm}(\eta) = r_{l,-m}(\eta)$ and $R_f > R_b$. The number of spherical harmonics $\mathbf{z}\mathbf{Y}_l^m(\theta, \phi)$ in the sum accommodates the detailed structure of the cutting process. With $\sin\alpha = R_b/R_f$, the range $\alpha \leqslant \theta \leqslant \pi$, $0 \leqslant \phi \leqslant 2\pi$ ensures that the rock surface matches the bore hole of radius R_b. If the spherical harmonic sum is empty then the rock-bit interface is modelled by a moving spherical cap of radius R_f and centre at a distance $|\Lambda^B(\eta)| - \sqrt{R_f^2 - R_b^2}$ vertically below the origin. Clearly the greater the magnitude of R_f the greater is the average curvature of the rock face in interaction with the drill-bit. The presence of spherical harmonics can be used to model the different cutting characteristics of tricone and polydiamond–crystalline drill-bits since they give rise to different observed patterns at the rock face during drilling. For drilling with contact between the drill-bit and surface $\Sigma(\eta)$ at $\sigma = 1$:

$$\mathbf{R}(1, \eta) = \mathbf{r}(\Theta(\eta), \Phi(\eta), \eta) \tag{74}$$

where the dynamic functions $\Theta(\eta)$, $\Phi(\eta)$ locate the position of the drill-bit on the rock surface $\Sigma(\eta)$. As the drill-bit moves on $\Sigma(\eta)$ the direction of the normal reaction varies and this in turn determines the magnitude of the frictional forces and torques on it. Let $\{\mathbf{t}_1, \mathbf{t}_2, \mathbf{N}\}$ be a Darboux basis adapted to this surface with unit normal direction $\mathbf{N}$:

$$\mathbf{t}_1 = \partial_\theta \mathbf{r}, \quad \mathbf{t}_2 = \partial_\phi \mathbf{r}, \quad \mathbf{N} = \mathbf{t}_1 \times \mathbf{t}_2 / |\mathbf{t}_1 \times \mathbf{t}_2|. \tag{75–77}$$

The orientation of $\mathbf{N}$ is chosen such that $\mathbf{N} \cdot \mathbf{k} > 0$ in the lower spherical cap. The motion of the bit in terms of $\Theta(\eta)$, $\Phi(\eta)$ (and the normal bit reaction force $\mathcal{F}_N^{bit}(\eta)$) follows by solving

$$\mu_{bit} \mathbf{R}(1, \eta)_{\eta\eta} = -\mathbf{n}(1, \eta) - \mu_{bit} g \mathbf{k} + \mathbf{F}^{bit}(\eta), \tag{78}$$

where

$$\mathbf{F}^{bit}(\eta) = \mathcal{F}_N^{bit}(\eta) \mathbf{N}(\Theta(\eta), \Phi(\eta)) + \mathbf{F}_T^{bit}(\eta) \tag{79}$$

and

$$\mathbf{F}_T^{bit}(\eta) = -\mathcal{F}_N^{bit}(\eta) \mathrm{H}(\mathcal{F}_N^{bit}(\eta)) \mu(|\mathbf{R}_\eta(1, \eta)|) \frac{\mathbf{R}_\eta(1, \eta)}{|\mathbf{R}_\eta(1, \eta)|} - k \mathbf{R}_\eta(1, \eta). \tag{80}$$

The function $\mu(|\mathbf{R}_\eta(1, \eta)|)$ is the prescribed coefficient of Coulombic bit-rock sliding friction as a function of relative lateral speed (with $\mathrm{sgn}(\mu(\nu)) = \mathrm{sgn}(\nu)$) and k is the coefficient of bit-rock viscous (Stokes) friction. The presence of the term $\mathrm{H}(\mathcal{F}_N^{bit}(\eta))$ where H is the Heaviside function ensures a contact friction interaction. The presence of the Stokes friction accommodates damping effect in the environment including the hydrodynamic effects of the drilling "mud". During evolution one solves for $\Theta(\eta)$, $\Phi(\eta)$ and $\mathcal{F}_N^{bit}(\eta)$. When $\mathcal{F}_N^{bit}(\eta) = 0$ for some η, physical contact between the drill-bit and the rock surface is lost and the boundary condition

$$\mu_{bit} \mathbf{R}(1, \eta)_{\eta\eta} = -\mathbf{n}(1, \eta) - \mu_{bit} g \mathbf{k} \tag{81}$$

becomes an equation for the three components of $\mathbf{R}(1, \eta)$ in space until motion intersects the rock surface again. This process can repeat and gives rise to the phenomenon of "bit bounce".

In order to implement the torque boundary condition at $\sigma = 1$ one supposes that the BHA stabilisers can be modelled by a constraint on the direction of the drill-string. Let $\mathbf{Q}$ be a fixed (time independent) unit vector in $\mathbf{R}^3$. (Then $\mathbf{V} - (\mathbf{V} \cdot \mathbf{Q})\mathbf{Q}$ is perpendicular to $\mathbf{Q}$ for any $\mathbf{V}$). Suppose the stabilisers on the BHA constrain the tangent to the drill-string in the direction $\mathbf{Q}$:

$$\mathbf{R}_\sigma(1, \eta) - (\mathbf{R}_\sigma(1, \eta) \cdot \mathbf{Q})\mathbf{Q} = 0. \tag{82}$$

Thus, with $\mathbf{Q} = -\mathbf{k}$:

$$\mathbf{R}_\sigma(1, \eta) \cdot \mathbf{i} = 0, \quad \mathbf{R}_\sigma(1, \eta) \cdot \mathbf{j} = 0. \tag{83, 84}$$

These stabiliser constraints are maintained by torques $\mathbf{L}_Q(\eta)$ on the BHA, where

$\mathbf{L}_Q(\eta) \cdot \mathbf{Q} = 0$. With $\mathbf{Q} = -\mathbf{k}$ this implies:

$$\mathbf{L}_Q(\eta) = L_x^{bit}(\eta)\mathbf{i} + L_y^{bit}(\eta)\mathbf{j}. \tag{85}$$

The torque boundary condition at the drill-bit must now include the constraining torque $\mathbf{L}_Q(\eta)$ as well as the bit-torque friction $\mathbf{L}^{bit}(\eta)$:

$$(\mathbf{J}^{bit}(\mathbf{w}))_\eta(1, \eta) = -\mathbf{m}(1, \eta) + \mathbf{L}^{bit}(\eta) + \mathbf{L}_Q(\eta), \tag{86}$$

where

$$\mathbf{L}^{bit}(\eta) = -\mathcal{F}_N^{bit}(\eta)\mathbf{N}(\eta)\mathrm{H}(\mathcal{F}_N^{bit}(\eta))\mathcal{F}(\mathbf{w}(1, \eta) \cdot \mathbf{N}(\eta)) \tag{87}$$

in terms of some prescribed bit-torque friction profile $\mathcal{F}$ with $\mathrm{sgn}(\mathcal{F}(\omega)) = \mathrm{sgn}(\omega)$. Thus the component of this equation in the direction $\mathbf{Q}$ must be satisfied:

$$(\mathbf{J}^{bit}(\mathbf{w}))_\eta(1, \eta) \cdot \mathbf{Q} = -\mathbf{m}(1, \eta) + \mathbf{L}^{bit}(\eta) \cdot \mathbf{Q}. \tag{88}$$

The components in the directions orthogonal to $\mathbf{Q}$ provide two equations for the components of the constraining torques $\mathbf{L}_Q(\eta)$: With $\mathbf{Q} = -\mathbf{k}$ these are:

$$L_x^{bit}(\eta) = (\mathbf{J}^{bit}(\mathbf{w}))_\eta(1, \eta) \cdot \mathbf{i} + \mathbf{m}(1, \eta) - \mathbf{L}^{bit}(\eta) \cdot \mathbf{i}, \tag{89}$$

$$L_y^{bit}(\eta) = (\mathbf{J}^{bit}(\mathbf{w}))_\eta(1, \eta) \cdot \mathbf{j} + \mathbf{m}(1, \eta) - \mathbf{L}^{bit}(\eta) \cdot \mathbf{j}. \tag{90}$$

5. INTERACTIONS WITH THE BORE CAVITY

During evolution the drill-string and drill-bit experience external forces and torques in addition to gravity since both are confined by the sides of the borehole and exposed to a dynamic hydrodynamic environment. In cases of excessive flexural excitation the drill-string or BHA may make contact at various times with the side wall of the borehole. Such impacts may not be impulsive for the drill-string. For example segments of differing length of the drill-string may move in contact with the wall for certain periods of time. In such cases a friction model for the body force in (1) can be developed which switches on along the segment of the drill-string when it is in contact with the wall. This approach is analogous to the frictional interaction of the drill-bit with the rock surface discussed in the previous section. An alternative and simpler approach (which also models the hydrodynamic environment in a crude manner) is to replace the confining cavity by a cylindrically symmetric confining potential $V(\mathbf{r}, \sigma)$. The structure of the potential is designed to produce a powerful confining force outside a range equal to the overgauge δ. For the drill-string $\delta \equiv \mathrm{R}_b - r_o$ whilst for the BHA it may be somewhat smaller. This models in a simple fashion the finite size of the drill-pipe and BHA and permits study of the drill-bit motion in the vicinity of the cavity wall. Thus the contribution $\mathbf{f}_c$ from the bore–cavity interaction to the external force $\mathbf{f}$ on the drill-string is defined by

$$\mathbf{f}_c(\sigma, \eta) = -\nabla(V)(\mathbf{R}(\sigma, \eta), \sigma) \tag{91}$$

in terms of some potential $V(\mathbf{r}, \sigma)$. A suitable potential is, for some $\delta(\sigma)$:

$$V(\mathbf{r}, \sigma) = \lambda_0\{(x/\delta(\sigma))^2 + (y/\delta(\sigma))^2\}^n, \tag{92}$$

where $\mathbf{r} = x\mathbf{i} + y\mathbf{j} + z\mathbf{k}$, the variable λ_0 determines the strength of the potential and the positive integer n determines its shape. In the simulations discussed below a value of $n = 8$ and a dimensionless $\delta = 1{\cdot}7 \times 10^{-5}$ is found to suitably model this interaction.

6. FRICTION

The Coulombic component of friction between macroscopic surfaces depends on the relative motion between surfaces in contact and the normal and tangential components of force with respect to such surfaces [20]. The magnitude of the normal force determines the magnitude of the "kinetic" frictional force or torque when the relative motion is non-zero and the instantaneous tangential force or torque determines the value of the "static" friction otherwise. It is well known that the value of this static friction is not a smooth function of the applied force or torque and that this often gives rise to relaxation phenomena or intermittent motion [19, 21, 24].

A system that exhibits motion in which certain degrees of freedom are constant for extended periods of time (ankylosis) can only be analysed in a piecewise manner. Various continuous approximations to the behaviour of Coulombic friction as a function of relative motion have been proposed in order to circumvent the need for a piecewise analysis. As long as the difference between the maximum static friction and the typical kinetic friction is not excessive such continuous approximations are found to yield acceptable alternatives [20, 23]. In the simulations considered in this article Coulombic friction at the drill-bit is simulated by the four parameter expression:

$$\mathcal{F}(v) = ABv(ab^2 + b^2 + B^2v^2)/(b^2 + B^2v^2)\sqrt{1 + B^2v^2}. \tag{93}$$

Note that

$$\operatorname*{Lim}_{v \mapsto \pm\infty} \mathcal{F}(v) = Av/|v| \tag{94}$$

and

$$\mathcal{F}(v) = ABv(1 + a) - AB^3v^3(ab^2 + b^2 + 2a)/2b^2 + O(v^5).$$

In Figure 2 the parameters $A > 0$, $B > 0$, $a > 0$, $b > 0$ have been chosen along with a typical "weight on bit" in order to display friction torque as a function of rotational speed typical of drill-bits in the field.

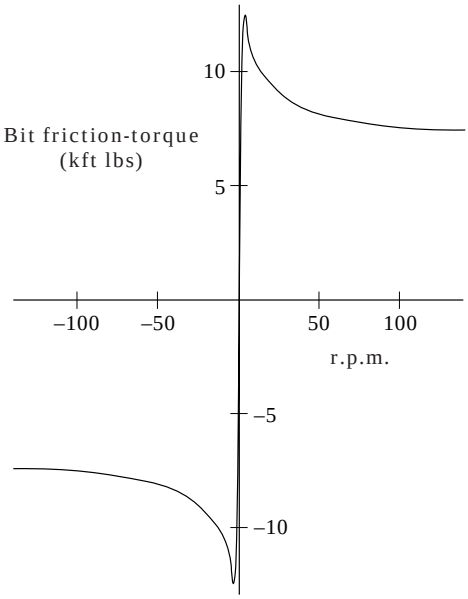

Figure 2. The excitation of torsional relaxation vibrations leading to the phenomena of slip–stick is determined by anti-damping characteristics induced by non-linear torque-friction between the active drill bit and the rock formation. The above profile simulates the frictional torque experienced in a typical field operation.

7. THE AXI-SYMMETRIC SECTOR

The equations (28–32) with constitutive relations (44–49) admit exact solutions with axial symmetry about the vertical of the form

$$\mathbf{d}_1(\sigma, \eta) = \cos(\Phi(\sigma, \eta))\mathbf{i} + \sin(\Phi(\sigma, \eta))\mathbf{j}, \tag{95}$$

$$\mathbf{d}_2(\sigma, \eta) = \sin(\Phi(\sigma, \eta))\mathbf{i} - \cos(\Phi(\sigma, \eta))\mathbf{j}, \tag{96}$$

$$\mathbf{d}_3(\sigma, \eta) = -\mathbf{k}, \quad \mathbf{R}(\sigma, \eta) = -(\sigma - g\sigma^2/2 + \zeta(\sigma, \eta))\mathbf{k}, \tag{97, 98}$$

where Φ and ξ satisfy the system of wave equations:

$$c^2\Phi_{\sigma\sigma} - \Phi_{\eta\eta} + \alpha_{m3}\Phi_{\eta\sigma\sigma} = 0, \quad \zeta_{\sigma\sigma} - \zeta_{\eta\eta} + \alpha_{n3}\zeta_{\eta\sigma\sigma} = 0. \tag{99, 100}$$

The parameter c defined by $c^2 = 1/(I_{11} + I_{22})$ may be rescaled to the speed of torsional wave propagation on the drill-string. Solutions to these equations may be expected to describe a straight vertical drill-string, free of lateral excitation and fluctuating interactions with the sides of the bore-hole.

In such an axi-symmetric configuration the boundary conditions (60–63) become

$$-\zeta_\sigma(0, \eta) - \alpha_{n3}\zeta_{\eta\sigma\sigma}(0, \eta) + F_z^{\mathrm{T}} - \mu_{top}g + \mu_{top}\zeta_{\eta\eta}(0, \eta) = 0, \tag{101}$$

$$J_{33}^{\mathrm{T}}\Phi_{\eta\eta}(0, \eta) - \Phi_\sigma(0, \eta) - \alpha_{m3}\Phi_{\sigma\sigma\eta}(0, \eta) - G_z^{\mathrm{T}} = 0, \tag{102}$$

$$\zeta_\sigma(1,\eta) - \alpha_{n3}\zeta_{\eta\sigma\sigma}(1,\eta) + F_z^B - \mu_{bit}g + \mu_{bit}\zeta_{\eta\eta}(1,\eta) = 0, \tag{103}$$

$$J_{33}^B\Phi_{\eta\eta}(1,\eta) + \Phi_\sigma(1,\eta) + \alpha_{m3}\Phi_{\sigma\sigma\eta}(1,\eta) - G_z^B = 0, \tag{104}$$

where $\mathbf{L}^{top} = G_z^T\mathbf{k}$, $\mathbf{L}^{bit} = G_z^B\mathbf{k}$, $\mathbf{F}^{top} = F_z^T\mathbf{k}$ and $\mathbf{F}^{bit} = F_z^B\mathbf{k}$.

In the following analysis of this section viscoelastic damping in the drill-string is neglected, $\alpha_{vscn3} = 0$, $\alpha_{vscn3} = 0$ and the torsional friction at the drill-bit is denoted by $G_z^B = -T_{\mathcal{W}}(\Phi_\eta(1,\ \eta))$ where $\mathcal{W}$ implies that the function $T_{\mathcal{W}}$ is parameterised by the magnitude of the normal reaction of the drill-bit on the rock.

The top-torque regulator

$$G_z^T = \kappa_p(\Omega_0 - \Phi_\eta(0,\eta)) + \kappa_i(\Omega_0\eta - \Phi(0,\eta)) \tag{105}$$

is designed to drive the system to the stationary solution

$$\hat{\Phi}(\sigma,\eta) = \Omega_0\eta - T_{\mathcal{W}}(\Omega_0)\sigma - T_{\mathcal{W}}(\Omega_0)/\kappa_i. \tag{106}$$

However this configuration may be unstable under small torsional fluctuations due to the non-linear structure of $T_{\mathcal{W}}$. The linearised torsional system is obtained by substituting

$$\Phi(\sigma,\eta) = \hat{\Phi}(\sigma,\eta) + \varepsilon\phi(\sigma,\eta) \tag{107}$$

into (99), (102) and (104). Then to order ε the system is determined by

$$\phi_{\eta\eta} - c^2\phi_{\sigma\sigma} = 0, \quad J_{33}^T\phi_{\eta\eta}(0,\eta) - \phi_\sigma(0,\eta) + \kappa\phi_\eta(0,\eta) + \kappa_i\phi(0,\eta), \tag{108, 109}$$

$$J_{33}^B\phi_{\eta\eta}(1,\eta) + \phi_\sigma(1,\eta) + T'_{\mathcal{W}}(\Omega_0)\phi_\eta(1,\eta) = 0. \tag{110}$$

Particular linearised modes correspond to solutions of the form:

$$\phi(\sigma,\eta) = [\phi_c\cosh(\mu\sigma/c) + \phi_s\sinh(\mu\sigma/c)]e^{\mu\eta}, \tag{111}$$

where μ is a complex root of the real transcendental equation:

$$c\tanh(\mu/c) = \frac{(J_{33}^T + J_{33}^B)\mu^2 + (\kappa_p + T'_{\mathcal{W}}(\Omega_0))\mu + \kappa_i}{J_{33}^TJ_{33}^B\mu^3 + (T'_{\mathcal{W}}(\Omega_0)J_{33}^T + \kappa_pJ_{33}^B)\mu^2 + (c^{-2} + \kappa_iJ_{33}^B + \kappa_pT'_{\mathcal{W}}(\Omega_0))\mu + \kappa_iT'_{\mathcal{W}}(\Omega_0)}. \tag{112}$$

This has infinitely many solutions for μ that are either real or occur in complex conjugate pairs. For each solution μ_j a non-trivial eigenmode with components $\phi_c(\mu_j)$ and $\phi_s(\mu_j)$ can be determined and the general solution is

$$\phi(\sigma,\eta) = \sum_{j=1}^{\infty} C_j[\phi_c(\mu_j)\cosh(\mu_j\sigma/c) + \phi_s(\mu_j)\sinh(\mu_j\sigma/c)]e^{\mu_j\eta}. \tag{113}$$

The complex constants C_j may be determined from the initial angular state and angular speed along the drill-string. An analysis of the location of the μ_j in the complex plane as a function of the parameters that appear in (112) offers guidance for stable drilling configurations (Re $\mu_j < 0$). If the "weight on bit" $\mathcal{W}$ is assumed to be the difference between the total weight suspended by the top cable and the average tension in this cable (independent of the axial vibrations in the drill-string and constant) then the axial and torsional equations decouple. The linear stability of the torsional sector can then be explored as a function of average "weight on bit" and the target rotary speed Ω_0 used by the torque motor controller [25]. A typical stability plot that exhibits the severity of local instabilities is shown in Figure 3.

It is clear that the high frequency torsional modes are given approximately by

$$\mu_n = \pm n\pi c \tag{114}$$

for large integers n. In the low frequency limit the roots approximately satisfy the fourth order polynomial.

$$(J_{33}^T\mu^2 + \kappa_p\mu + 1 + \kappa_i)(J_{33}^B\mu^2 + T'_{\mathcal{W}}(\Omega_0)\mu + 1) - 1 = 0. \tag{115}$$

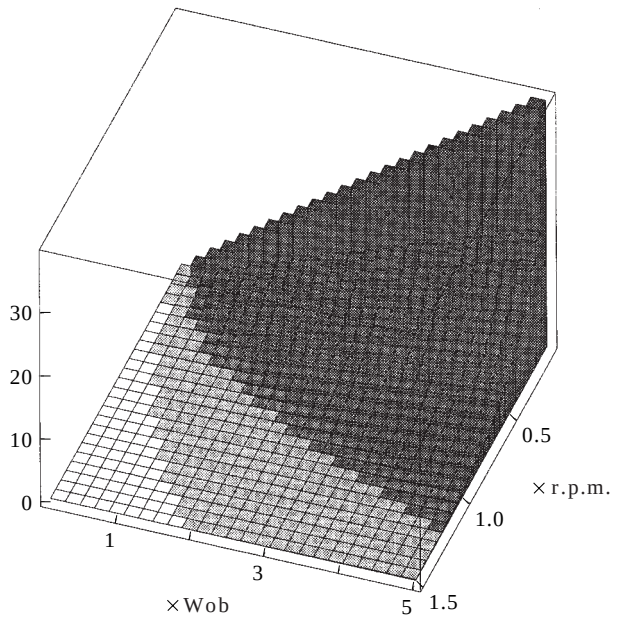

Figure 3. The active drill system can excite an infinite number of characteristic vibrational modes. The frequency and lifetime of mode instabilities are encoded in the roots of the characteristic system associated with a linearisation about a stationary target configuration. The figure displays the pure torsional vibrational spectrum for typical base parameters as a function of target rotary speed and "weight-on-bit" (wob) The scales on the horizontal axes are chosen so that the point (1,1) corresponds to a value of 100 kN for the weight on bit and 90 r.p.m. for the target rotary speed. Each axis is then scaled in terms of these units. The grey domains indicate the absence of excitable unstable modes and correspond to "safe" drilling configurations. The vertical blocks indicate the presence of unstable torsional vibrations. The height of each block indicates the reciprocal of the life-time (in seconds) of the most unstable mode in this domain.

This corresponds to the limit in which the propagation of linearised torsional waves along the drill-string is assumed to be instantaneous,

$$\Phi(\sigma, \eta) \simeq \alpha(\eta) + \sigma(\beta(\eta) - \alpha(\eta)) \tag{116}$$

and the system becomes modelled by a pair of torsional pendulums [26] coupled by a torsional spring and with frictional torque $T_{\mathcal{W}}(\beta_\eta) = \mathcal{W}\mathcal{F}(\beta_\eta)$:

$$J^T_{33}\alpha_{\eta\eta}(\eta) + \alpha(\eta) - \beta(\eta) - G^T_z = 0, \quad J^B_{33}\beta_{\eta\eta}(\eta) - \alpha(\eta) + \beta(\eta) - G^B_z = 0. \tag{117, 118}$$

The linearised axi-symmetric sector is a useful guide in setting up simulations with the non-linear equations (117) and (118). These display the manner in which the instabilities manifest themselves as torsional relaxation oscillations (Figure 4).

However the boundary conditions at $\sigma = 1$ provide an inevitable coupling between the axial and torsional sectors since the reaction at the bit $\mathcal{W} \equiv F^B_z(\eta)$ is dynamic. This influences the torque friction at the drill-bit and couples equations (99) and (100) through $T_{\mathcal{W}}$ in (103) and (104). A numerical simulation based on the techniques to be introduced in the next section reveals that assuming the axial and torsional sectors to be independent becomes increasingly suspect as the average "weight on bit" increases during the drilling process [27].

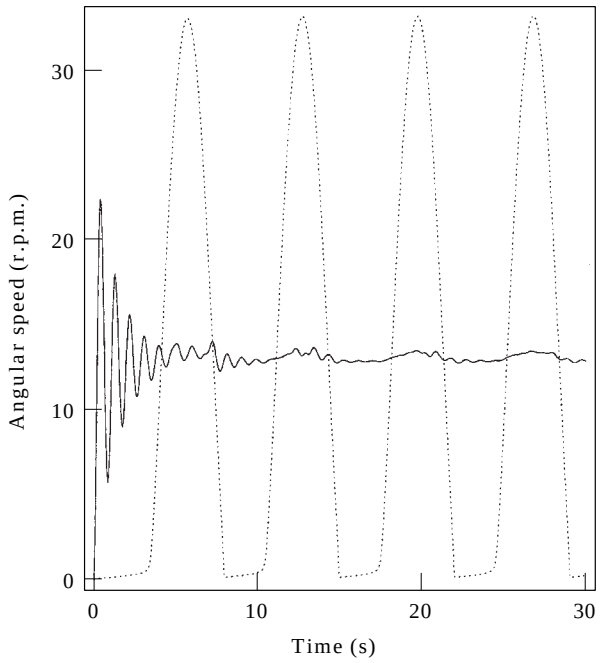

Figure 4. This figure displays the angular speed of the top-drive (full curve) and drill-bit (dotted curve) in r.p.m. as a function of time (s) from solutions to equations (117) and (118). The drill-bit clearly exhibits torsional relaxation oscillations becoming intermittently arrested every few seconds despite the top-drive maintaining a steady rotary speed after initial transient fluctuations.

8. REDUCTION TO DIFFERENTIAL DELAY EQUATIONS

The neglect of retardation effects due to the continuum nature of the drill-string implies that simulations based on the equations (117) and (118) above may misrepresent torsional relaxation vibrations and their interaction with the axial motions of the drill-string. In particular the duration of torsional "stick" is expected to be influenced by both these features. To investigate this, one is confronted with solving the partial differential equations (99) and (100) subject to the time dependent boundary conditions (101–104). The traditional approach to this problem is via some spatial discretisation or finite element approximation that reduces the partial differential equations to a finite system of coupled ordinary differential equations. However for the axially symmetric configurations under discussion the general solution of the linear wave equations can be expressed in terms of functions of a single variable and an alternative approach is to substitute these solutions into the boundary conditions. This transforms the initial boundary value problem for the wave equations into an initial problem for a finite system of *retarded differential–difference equations*. That the original Cauchy problem can indeed be replaced by the integration of such a system relies on being able to translate the Cauchy data for the partial differential wave equations into suitable initial data for the retarded differential–difference system. The method used to effect this is outlined in Appendix 2. The result is that the Cauchy problem for n linear wave equations of the form

$$\ddot{\phi}_k - \beta_k^2 \phi_k'' = 0, \quad k = 1, \ldots, n, \tag{119}$$

with in general different propagation constants $\{\beta_k\}$, subject to coupled dynamical boundary conditions (that may themselves be coupled to degrees of freedom $F_j(\eta)$ satisfying another ordinary differential system), can be replaced by a system of non-linear retarded differential–difference equations of the form:

$$\mathbf{X}_\eta(\eta) = \mathbf{F}(\mathcal{F}_j(\eta - 1/\beta_j), \quad F_k(\eta)), \tag{120}$$

where $\{\mathbf{X}\} \equiv \{\mathcal{F}_j, F_j\}$ is specified (via the Cauchy data for ϕ_k) on $-\min\{1/\beta_j\} \leqslant \eta \leqslant 0$. Solutions $\mathbf{X}(\eta)$ for $\eta > 0$ permit construction of $L_k(\eta)$ and $R_k(\eta)$ where

$$\phi_k(\sigma, \eta) = L_k(\sigma + \beta_k \eta) + R_k(\sigma - \beta_k \eta). \tag{121}$$

Methods [28, 29] for solving (120) involve "leap frogging" data on finite intervals forward in time. One of the advantages of this approach is that fine structure in the solutions found by numerical simulation is limited only by convergence criteria on the temporal discretisation step-length. The method is therefore ideally suited to explore the effects of travelling waves in the drill-string in the presence of relatively high frequency axial vibrations. As a result of taking into account torsional retardation effects due to the finite size of the drill-string, torsional "slip-stick" phases generally exhibit *longer* periods of "stick" than in similar situations where the continuum nature of the drill-

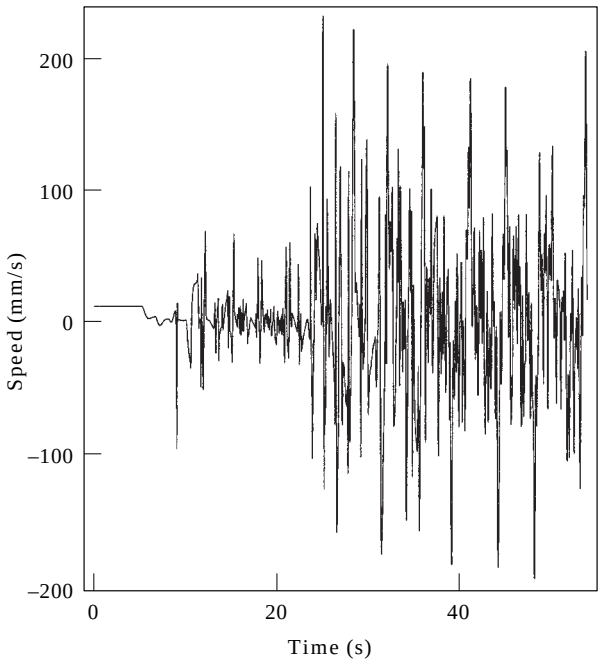

Figure 5. Variation of the vertical oscillatory component of the speed of the drill-bit as a function of time (s) as described by solution of the delay–differential system 120. The increase in axial vibration is induced by a change of rock lithology from sandstone to granite.

string is ignored. This is readily understood in terms of the finite time required to exchange torsional kinetic energy between the top-drive and BHA along the drill-string. The intensity of axial vibrations that can arise in the presence of torsional wave excitation of the drill-string may be estimated from Figures 5–8. These are produced from a single simulation based on the techniques given in Appendix 2 for the solution of the system of equations (120).

9. FLEXURAL STABILITY

The drill-string is also prone to lateral excitations as a perturbation analysis about the static configuration (50), (51), (55) reveals. Substituting

$$\mathbf{R}(\sigma, \eta) = \varepsilon X(\sigma, \eta)\mathbf{i} + (g\sigma^2/2 - \sigma + \varepsilon Z(\sigma, \eta))\mathbf{k}, \tag{122}$$

$$\mathbf{d}_1 = \mathbf{i} + \varepsilon\Theta(\sigma, \eta)\mathbf{k}, \quad \mathbf{d}_2 = -\mathbf{j}, \quad \mathbf{d}_3 = -\mathbf{k} + \varepsilon\Theta(\sigma, \eta)\mathbf{i} \tag{123–125}$$

into (28–32), (44–49) yields equations for axial, lateral and flexural waves:

$$(\partial^2/\partial\eta^2)Z(\sigma, \eta) - (\partial^2/\partial\sigma^2)Z(\sigma, \eta) - \alpha_{n3}(\partial^3/\partial\eta\partial\sigma^2)Z(\sigma, \eta) = 0, \tag{126}$$

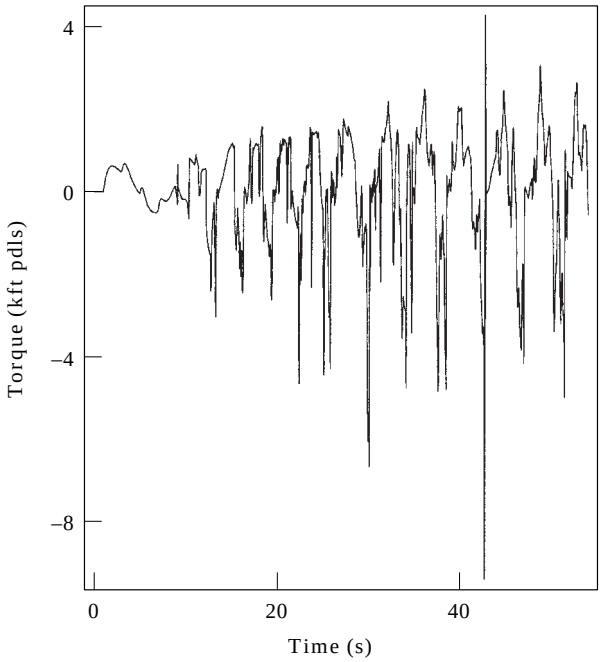

Figure 6. Variation of the total torque (kft-pdls) experienced by the drill-bit as a function of time (s) as described by a solution of the delay-differential system 120. The variation is induced by a combination of axial activity in the drill-string producing a fluctuating force on the drill-bit and torsional relaxation oscillations induced by the frictional torque between the drill-bit and the rock face.

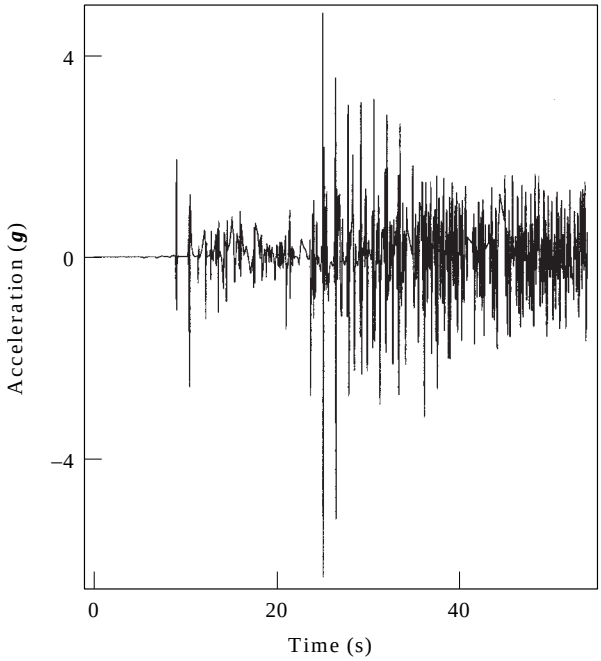

Figure 7. Variation of the vertical acceleration (in g) of the drill-bit as a function of time (s) as described by solution of the delay–differential system 120. The increase in axial vibration is induced by a change of rock lithology from sandstone to granite.

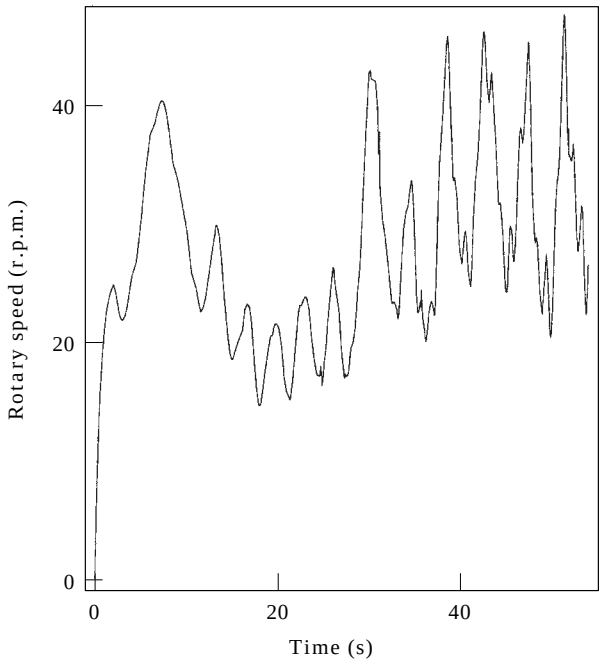

Figure 8. Variation of rotary speed (r.p.m.) of the top-drive speed controller as a function of time (s) as described by a solution of the delay–differential system (120). The controller is set to attain a target speed of 30 r.p.m. but as a result of severe torsional relaxation oscillations is unable to absorb torsional kinetic energy incident on the top rotary table. This is the type of destructive behaviour that additional top-torque controllers are designed to ameliorate.

$$\Theta(\sigma,\eta)(\sigma g-1)\kappa(\chi+\sigma g-\chi\sigma g)-\kappa\chi\alpha_{n1}(\sigma g-1)^2(\partial/\partial\eta)\Theta(\sigma,\eta)$$
$$-\alpha_{n1}\kappa\chi(\sigma g-1)(\partial^2/\partial\eta\partial\sigma)X(\sigma,\eta)+I_{22}\alpha_{m2}(\partial^3/\partial\eta\partial\sigma^2)\Theta(\sigma,\eta)$$
$$+I_{22}(\partial^2/\partial\sigma^2)\Theta(\sigma,\eta)-I_{22}(\partial^2/\partial\eta^2)\Theta(\sigma,\eta)+\kappa(\chi+\sigma g-\chi\sigma g)(\partial/\partial\sigma)X(\sigma,\eta)$$
$$=0, \tag{127}$$

$$\Theta(\sigma,\eta)g(\chi-1)+\chi(\partial^2/\partial\sigma^2)X(\sigma,\eta)+\chi\alpha_{n1}(\partial/\partial\eta\Theta(\sigma,\eta))g$$
$$+\alpha_{n1}\chi(\sigma g-1)(\partial^2/\partial\eta\partial\sigma)\Theta(\sigma,\eta)-(\chi+\sigma g-\chi\sigma g)(\partial/\partial\sigma)\Theta(\sigma,\eta)$$
$$-(\partial^2/\partial\eta^2)X(\sigma,\eta)+\chi\alpha_{n1}(\partial^3/\partial\eta\partial\sigma^2)X(\sigma,\eta)=0. \tag{128}$$

If the viscoelastic damping and gravitational weight terms proportional to g are neglected equations (139) and (140) may be decoupled resulting in the traditional Euler–Bernoulli–Kelvin beam equation for small lateral deflections [30–32]:

$$I_{22}\chi(\partial^4/\partial\sigma^4)X(\sigma,\eta)+\chi\kappa(\partial^2/\partial\eta^2)X(\sigma,\eta)$$
$$-I_{22}(1+\chi)(\partial^4/\partial\sigma^2\partial\eta^2)X(\sigma,\eta)+I_{22}(\partial^4/\partial\eta^4)X(\sigma,\eta)=0. \tag{129}$$

As in the section above, the linearised boundary conditions lead to a coupled root analysis that determines the nature of lateral and axial stability about the static configuration.

10. ROTARY-SYNCHRONOUS WHIRL

The stability analysis can be extended to include axial, lateral, torsional and flexural excitations of the drill-string. To this end it is useful to parameterise the orthonormal directors by the three Euler angles ϕ, θ, ψ:

$$\begin{aligned}\mathbf{d}_1(\sigma,\eta) = {} & (\cos(\psi(\sigma,\eta))\cos(\theta(\sigma,\eta))\cos(\phi(\sigma,\eta)) - \sin(\psi(\sigma,\eta))\sin(\phi(\sigma,\eta)))\mathbf{i} \\ & + (\cos(\psi(\sigma,\eta))\cos(\theta(\sigma,\eta))\sin(\phi(\sigma,\eta)) + \sin(\psi(\sigma,\eta))\cos(\phi(\sigma,\eta)))\mathbf{j} \\ & - \cos(\psi(\sigma,\eta))\sin(\theta(\sigma,\eta))\mathbf{k}, \end{aligned} \tag{130}$$

$$\begin{aligned}\mathbf{d}_2(\sigma,\eta) = {} & (-\sin(\psi(\sigma,\eta))\cos(\theta(\sigma,\eta))\cos(\phi(\sigma,\eta)) - \cos(\psi(\sigma,\eta))\sin(\phi(\sigma,\eta)))\mathbf{i} \\ & + (-\sin(\psi(\sigma,\eta))\cos(\theta(s,t))\sin(\phi(\sigma,\eta)) + \cos(\psi(\sigma,\eta))\cos(\phi(s,t)))\mathbf{j} \\ & + \sin(\psi(\sigma,\eta))\sin(\theta(\sigma,\eta))\mathbf{k}, \end{aligned} \tag{131}$$

$$\mathbf{d}_3(\sigma,\eta) = \sin(\theta(\sigma,\eta))\cos(\phi(\sigma,\eta))\mathbf{i} + \sin(\theta(\sigma,\eta))\sin(\phi(\sigma,\eta))\mathbf{j} + \cos(\theta(\sigma,\eta))\mathbf{k}. \tag{132}$$

Of particular relevance to drill-string dynamics are the so called whirling excitations in which, besides flexural and torsional motions, the transverse components of the line of centroids of the drill-string are stationary in a vertical plane rotating about a vertical axis [16]. If the system is unstable under whirling perturbations about the axisymmetric configurations discussed above then the drill-string can impact with the borehole at different points along its length triggering lateral wave motion that can generate bit-bounce. Attempts to rectify this can then set up a new cycle of the torsional instabilities discussed above. (This phenomenon is explored in section 13.)

A whirling perturbation about the static configuration takes the form

$$\mathbf{R}(\sigma,\eta) = \varepsilon X(\sigma)\cos(\Omega\eta)\mathbf{i} + \varepsilon X(\sigma)\sin(\Omega\eta)\mathbf{j} + (g\sigma^2/2 - \sigma + \varepsilon Z(\sigma,\eta))\mathbf{k}, \tag{133}$$

where the lateral displacement $X(\sigma)$ takes place in a vertical plane rotating about $\mathbf{k}$ with fixed angular speed, Ω. If this speed coincides with the steady rotary speed of the drill-string about the Euler angle ϕ is perturbed according to

$$\phi(\sigma,\eta) = \Omega\eta + \varepsilon\Phi(\sigma,\eta), \tag{134}$$

then the motion is known as rotary-synchronous whirl. A consistent linearisation now follows with

$$\psi(\sigma,\eta) = \pi + \varepsilon\Psi(\sigma,\eta), \quad \theta(\sigma,\eta) = \pi + \varepsilon\Theta(\sigma). \tag{135, 136}$$

The perturbed directors take the form:

$$\mathbf{d}_1(\sigma,\eta) = (\cos(\Omega\eta) + \varepsilon\sin(\Omega\eta)(\Psi(\sigma,\eta)) - \Phi(\sigma,\eta))\mathbf{i} + (\sin(\Omega\eta) - \varepsilon\cos(\Omega\eta)(\Psi(\sigma,\eta)) - \Phi(\sigma,\eta))\mathbf{j} - \varepsilon\Theta(\sigma)\mathbf{k}, \quad (137)$$

$$\mathbf{d}_2(\sigma,\eta) = (\sin(\Omega\eta) + \varepsilon\cos(\Omega\eta)(\Phi(\sigma,\eta)) - \Psi(\sigma,\eta))\mathbf{i} - (\cos(\Omega\eta) + \varepsilon\sin(\Omega\eta)(\Phi(\sigma,\eta)) - \Psi(\sigma,\eta))\mathbf{j} \quad (138)$$

$$\mathbf{d}_3(\sigma,\eta) = -\varepsilon\Theta(s)\cos(\Omega\eta)\mathbf{i} - \varepsilon\Omega(s)\sin(\Omega\eta)\mathbf{j} - \mathbf{k} \quad (139)$$

Substituting these equations into (28–32) and (38–43) yields equations for the perturbations $X(\sigma)$, $Z(\sigma,\ \eta)$, $\Theta(\sigma)$ and the difference $\Phi(\sigma,\ \eta) - \Psi(\sigma,\ \eta)$. In the absence of viscoelastic damping these take the form:

$$(\partial^2/\partial\sigma^2)Z(\sigma,\eta) - (\partial^2/\partial\eta^2)Z(\sigma,\eta) = 0, \quad (140)$$

$$(I_{11} + I_{22})(\partial^2/\partial\eta^2)(\Phi - \Psi)(\sigma,\eta) - (\partial^2/\partial\sigma^2)(\Phi - \Psi)(\sigma,\eta) = 0, \quad (141)$$

$$((1-\chi)g\sigma + \chi)\frac{\mathrm{d}}{\mathrm{d}\sigma}\Theta(\sigma) + (1-\chi)g\Theta(\sigma) + X(\sigma)\Omega^2 + \chi\frac{\mathrm{d}^2}{\mathrm{d}\sigma^2}X(\sigma) = 0, \quad (142)$$

$$I_{22}(\mathrm{d}^2/\mathrm{d}\sigma^2)\Theta(\sigma) - ((1-\chi)g\kappa\sigma + \kappa\chi)(\mathrm{d}/\mathrm{d}\sigma)X(\sigma) - ((\chi-1)g^2\kappa\sigma^2 + (1-2\chi)g\kappa\sigma + \kappa\chi + I_{22}\Omega^2)\Theta(\sigma) = 0. \quad (143)$$

The system thus exhibits linearised torsional and axial wave propagation and gravity modulated flexural and Euler–Bernoulli–Kelvin bending modes. As before these modes are coupled via the linearised boundary conditions. Although a linearised analysis can be a valuable guide to the domains of stability free of axial and torsional instabilities in the presence of synchronous whirl the above modes of excitation by no means exhaust the space of linearised solutions in this vicinity. For example a class of purely oscillatory vibrations can be obtained from the perturbations

$$\mathbf{R}(\sigma,\eta) = \varepsilon X(\sigma)\sin(\omega\eta)\mathbf{i} + (g\sigma^2/2 - \sigma + \varepsilon Z(\sigma)\sin(\omega\eta))\mathbf{k}, \quad (144)$$

$$\psi(\sigma,\eta) = \pi, \quad \phi(\sigma,\eta) = \varepsilon\Phi(\sigma)\sin(\omega\eta), \quad \theta(\sigma,\eta) = \pi + \varepsilon\Theta(\sigma)\sin(\omega\eta), \quad (145\text{–}147)$$

$$\mathbf{d}_1(\sigma,\eta) = \mathbf{i} + \varepsilon\sin(\omega\eta)\Phi(\sigma)\mathbf{j} - \varepsilon\sin(\omega\eta)\Theta(\sigma)\mathbf{k}, \quad (148)$$

$$\mathbf{d}_2(\sigma,\eta) = -\mathbf{j} + \varepsilon\sin(\omega\eta)\Phi(\sigma)\mathbf{i}, \quad (149)$$

$$\mathbf{d}_3(\sigma,\eta) = -\mathbf{k} - \varepsilon\sin(\omega\eta)\Theta(\sigma)\mathbf{i}, \quad (150)$$

where the shape functions $X(\sigma)$, $Z(\sigma)$, $\Phi(\sigma)$ and $\Theta(\sigma)$ satisfy the ordinary system of differential equations:

$$(1-\chi)g\Theta(\sigma)+(1-\chi)(\mathrm{d}/\mathrm{d}\sigma\Theta(\sigma))g\sigma+X(\sigma)\omega^2$$
$$+\chi(\mathrm{d}/\mathrm{d}\sigma)\Theta(\sigma)+\chi(\mathrm{d}^2/\mathrm{d}\sigma^2)X(\sigma)=0, \tag{151}$$

$$(1-\chi)\kappa\Theta(\sigma)g^2\sigma^2+((2\chi-1)\kappa\Theta(\sigma)+\kappa(\chi-1)(\mathrm{d}/\mathrm{d}\sigma)X(\sigma))g\sigma$$
$$+\Theta(\sigma)(I_{22}-\kappa\chi\omega^2)-\kappa\chi(\mathrm{d}/\mathrm{d}\sigma)X(\sigma)+I_{22}(\mathrm{d}^2/\mathrm{d}\sigma^2)\Theta(\sigma), \tag{152}$$

$$\omega^2(I_{11}+I_{22})\Phi(\sigma)+(\mathrm{d}^2/\mathrm{d}\sigma^2)\Phi(\sigma)=0, \quad \omega^2 Z(\sigma)+(\mathrm{d}^2/\mathrm{d}\sigma^2)Z(\sigma)=0 \tag{153, 154}$$

Which mode in any of the perturbations above is dominant depends to a great extent on the initial conditions and the manner in which the drilling process is controlled in time. Guided by the linearised stability analysis this can be explored by a non-perturbative approach based on a discretisation of the field equations and their boundary conditions. Although recourse to numerical simulation is then inevitable, new insight can be gained on the role played by the initial conditions in the dynamic evolution of the system. Attention is now turned to the establishment of a suitable discretisation of the model which can be used to explore non-perturbative simulations for general configurations.

11. REDUCTION TO THE METHOD OF LINES

The integration of the equations (1, 2, 5–7, 11, 12) with (in general dynamic) boundary conditions poses a number of problems. The large disparity between magnitudes of the dimensionless parameters in these equations, (appropriate for a steel drill-string) means that any discretization will inevitable lead to a "stiff" system. Furthermore any discretization of the equations of motion should maintain the preservation of the orthonormality between the directions $\{\mathbf{d}_k\}$ during the evolution. The Euler angle parameterisation of $\{\mathbf{d}_k\}$ is unsuitable in this respect due to the presence of co-ordinate singularities that may not properly cancel in any numerical approximation. The presence of the Heaviside functions in some of the boundary conditions suggests that the evolution requires a piecewise construction. In any discretization to a system of ordinary differential equations, this raises a delicate question of convergence when using numerical algorithms that are based on approximating solutions satisfying a Lipschitz condition. Finally there is the question of ensuring that the choice of initial conditions is compatible with the boundary conditions for the system.

The first problem is addressed by adopting a spatial discretisation based on a truncated Fourier representation of the system and using semi-implicit techniques [33] to integrate the resulting system of ordinary differential equations. This offers the ability to experiment with different "stiff" numerical integrators and is most appropriate for the discretization of a quasilinear system of partial differential equations such as (1, 2, 5–7, 11, 12).

The preservation of the orthonormality of the moving director basis is effectively maintained by appending to the equations of motion the algebraic orthonormality conditions

$$\mathbf{d}_i(\sigma, \eta) \cdot \mathbf{d}_j(\sigma, \eta) = \delta_{ij}, \tag{155}$$

for $1 \leqslant i, j \leqslant 3$ thereby transforming the problem into a system of PDAE's (partial differential–algebraic equations). In order to pursue this approach care must be exercised in the discretization to ensure that the approximating ordinary differential–algebraic (ODAE) problem has index one [34].

One approach to handling discontinuous boundary conditions is to regularise terms such as $f(\eta)\mathrm{H}(f(\eta))$ by replacing them by suitable smooth approximations. Such regularizations have been shown to be quite effective in approximating Coulomb friction under certain conditions [23] although considerable care is required to adapt the regularization scales involved* in dynamical simulations. In the simulations discussed in section 13 such regularisations are not required.

The question of compatibility of initial data with the boundary conditions is solved at the level of the spatially discretized system by using a Fourier representation of the data. This has the added advantage that fast Fourier transform algorithms can then be employed.

In the following section a brief outline is given of how these techniques are implemented in practice.

12. DISCRETIZATION

Suppose, for some integer N, $a : \mathbf{Z}_N \mapsto \mathbf{C}$ is a complex function defined on the integers modulo N. Thus $a_p = a_{p+N}$ for $0 \leqslant p \leqslant N-1$ say. Recall that the discrete Fourier transform of a is given by

$$h_\ell = \sum_{p=0}^{N-1} a_p \exp\left(\mathrm{i}\frac{2\pi p\ell}{N}\right), \tag{156}$$

for $0 \leqslant p \leqslant N-1$. The transform is now N-periodic $h_\ell = h_{\ell+N}$ and it follows that

$$a_p = \frac{1}{N}\sum_{\ell=0}^{N-1} h_\ell \exp\left(-\mathrm{i}\frac{2\pi p\ell}{N}\right). \tag{157}$$

where $0 \leqslant \ell \leqslant N-1$. Since one is concerned with real valued h_ℓ $\Re(a_{N-p}) = \Re(a_p), \Im(a_{N-p}) = -\Im(a_p)$ and hence for N even

*The scale of the simple regularization $\frac{1}{2}(f(\eta) + \sqrt{f(\eta)^2 + \varepsilon^2})$ for $f(\eta)\mathrm{H}(f(\eta))$ is set by the small parameter ε.

$$h_\ell = \sum_{p=0}^{N-1}\left[\Re(a_p)\cos\left(\frac{2\pi p\ell}{N}\right) - \Im(a_p)\sin\left(\frac{2\pi p\ell}{N}\right)\right]$$

$$= \Re(a_0) + 2\sum_{p=1}^{N/2-1}\left[\Re(a_p)\cos\left(\frac{2\pi p\ell}{N}\right) - \Im(a_p)\sin\left(\frac{2\pi p\ell}{N}\right)\right] + \Re(a_{N/2})\cos(\pi\ell). \tag{158}$$

By contrast if $u: S^1 \mapsto \mathbf{C}$ is a complex function on the unit circle it may be represented as

$$u(\theta) = \sum_{k=-\infty}^{k=\infty} \tilde{u}_k \exp(\mathrm{i}k\theta), \tag{159}$$

where

$$\tilde{u}_k = \frac{1}{2\pi}\int_0^{2\pi} u(\theta)\exp(-\mathrm{i}k\theta)\,\mathrm{d}\theta. \tag{160}$$

If u is sampled at points $\theta_j = 2\pi j/N$ for $0 \leqslant j \leqslant N-1$ and the data $u(\theta_j)$ used to define

$$\tilde{u}_k^N = \frac{1}{N}\sum_{j=0}^{N-1} u(\theta_j)\exp(-\mathrm{i}k\theta_j), \tag{161}$$

it follows that

$$\tilde{u}_k^N = \tilde{u}_k + \tilde{u}_{k\pm N} + \tilde{u}_{k\pm 2N} + \cdots, \tag{162}$$

This result implies that for sufficiently large N the discrete Fourier transform $\tilde{u}_k^N$ of a sampled sequence $\{u(\theta_j)\}$ of a smooth periodic function provides a discretisation of u that approximates $\tilde{u}_k$ for $0 \leqslant k \leqslant N-1$.

For a real periodic function h defined on $0 \leqslant \sigma \leqslant 1$ let

$$h_\ell = h(\sigma_\ell), \tag{163}$$

where

$$\sigma_\ell = 1/2N + \ell/N \tag{164}$$

for integers $1 \leqslant \ell \leqslant N$. In terms of

$$\hat{\ell}(\sigma) = N\sigma - \tfrac{1}{2}, \tag{165}$$

the data $\{h(\sigma_\ell)\}$ gives rise to a periodic extension $\hat{h}$ of h

$$\hat{h}(\sigma) := \Re(a_0) + 2\sum_{p=1}^{N/2-1}\left[\Re(a_p)\cos\left(\frac{2\pi p\hat{\ell}(\sigma)}{N}\right) - \Im(a_p)\sin\left(\frac{2\pi p\hat{\ell}(\sigma)}{N}\right)\right]$$

$$+ \Re(a_{N/2})\cos(\pi\hat{\ell}(\sigma)) = \sum_{p=1}^{N/2}\hat{a}_p\sin(2\pi p\sigma) + \sum_{p=0}^{N/2-1}\hat{b}_p\cos(2\pi p\sigma), \qquad (166)$$

where

$$\hat{b}_0 = \Re(a_0), \quad \hat{a}_{N/2} = \Re(a_{N/2}), \qquad (167, 168)$$

$$\hat{b}_p = 2\Re(a_p)\cos(\pi p/N) + 2\Im(a_p)\sin(\pi p/N) \quad \text{for} \quad 1 \leqslant p \leqslant N/2 - 1 \qquad (169)$$

$$\hat{a}_p = 2\Re(a_p)\sin(\pi p/N) + 2\Im(a_p)\cos(\pi p/N) \quad \text{for} \quad 1 \leqslant p \leqslant N/2 - 1. \qquad (170)$$

The basic assumption now is that some function $f(\sigma)$ representing initial data (which of course need not be periodic on $0 \leqslant \sigma \leqslant 1$) be approximated by such an extension plus a polynomial in σ of suitable degree. Defining

$$h(\sigma) = f(\sigma) - \sum_{q=1}^{Q} c_q(2\sigma - 1)^q, \qquad (171)$$

for some positive integer Q, let the coefficients of the polynomial c_q be given by the Q equations

$$D^j(h)(0) = D^j(h)(1), \qquad (172)$$

for $0 \leqslant j \leqslant Q - 1$. If f is smooth these conditions mean that at least h and its first $Q - 1$ derivatives are smooth functions on the unit interval with periodic Fourier extensions. Thus with $N = 2^m$ for some positive integer m, the results above enable one to approximate f by

$$\hat{f}(\sigma) := \hat{h}(\sigma) + \sum_{q=1}^{Q} c_q(2\sigma - 1)^q, \qquad (173)$$

using fast Fourier transform algorithms. The choice of Q is dictated by the degree of smoothness of the initial data and the extent to which it is desired that $\hat{f}$ be compatible with the boundary conditions and equations of motion (see below).

In order to succinctly present the discretisation algorithm used to reduce the partial differential equations (1, 2, 5–7, 11, 12) with boundary conditions to an ordinary differential system it is convenient to denote all functions of the two independent variables σ and η by $\{\phi_k\}$ $(1 \leqslant k \leqslant K)$. Furthermore dynamic functions of η that enter into the boundary conditions at $\sigma = 0$ and $\sigma = 1$ are denoted collectively by $\{\Lambda_0^r(\eta)\}$, $1 \leqslant r \leqslant E_0$ and $\{\Lambda_1^u(\eta)\}$, $1 \leqslant u \leqslant E_1$ respectively.

A system of K coupled partial differential equations is then denoted collectively by

$$\mathcal{P}^j(\ldots, \partial_\sigma^m \partial_\eta^n \phi_k(\sigma, \eta), \ldots) = 0, \tag{174}$$

it being understood that the displayed argument is generic; not every equation need involve all functions of the two independent variables. In a similar way the boundary conditions may be written as:

$$\mathcal{F}_0^a(\ldots, \partial_\sigma^m \partial_\eta^n \phi_k(0, \eta), \ldots, \partial_\eta^s \Lambda_0^r(\eta), \ldots) = 0, \tag{175}$$

$$\mathcal{F}_1^b(\ldots, \partial_\sigma^m \partial_\eta^n \phi_k(1, \eta), \ldots, \partial_\eta^v \Lambda_1^u(\eta), \ldots) = 0, \tag{176}$$

where $1 \leqslant a \leqslant H_0$, $1 \leqslant b \leqslant H_1$ and $H_0 + H_1 = H$, it being understood again that the arguments are generic. The basic spatial discretisation rule now follows from the discussion above. Each ϕ_k is approximated by a polynomial in σ_ℓ plus a discrete Fourier series with η dependent coefficients:

$$\hat{\phi}_k(\sigma_\ell, \eta) = \sum_{p=1}^{N/2} A_{kp}(\eta) \sin(2\pi p \sigma_\ell) + \sum_{p=0}^{N/2-1} B_{kp}(\eta) \cos(2\pi p \sigma_\ell)$$

$$+ \sum_{q=1}^{Q_k} C_{kq}(\eta)(2\sigma_\ell - 1)^q, \tag{177}$$

where $0 \leqslant \ell \leqslant N + 1$ and the $N + 2$ sampled spatial points σ_ℓ are defined by $\sigma_0 = 0$, $\sigma_{N+1} = 1$ and $\sigma_\ell = 1/2N + \ell/N$ for $1 \leqslant \ell \leqslant N$ so that the partial differential equations are sampled at the two end points $\sigma = 0$ and $\sigma = 1$ as well as at N interior points. In terms of

$$\hat{\mathcal{P}}^j_\ell(\ldots, \partial_\eta^n A_{kp}(\eta), \ldots, \partial_\eta^n B_{kp}(\eta), \ldots, \partial_\eta^n C_{kq}(\eta), \ldots)$$

$$= \mathcal{P}^j(\ldots, \partial_\sigma^m \partial_\eta^n \phi_k(\sigma_\ell, \eta), \ldots), \tag{178}$$

$$\hat{\mathcal{F}}_0^a(\ldots, \partial_\eta^n A_{kp}(\eta), \ldots, \partial_\eta^n B_{kp}(\eta), \ldots, \partial_\eta^n C_{kq}(\eta), \ldots, \partial_\eta^s \Lambda_0^r(\eta), \ldots)$$

$$= \mathcal{F}_0^a(\ldots, \partial_\sigma^m \partial_\eta^n \hat{\phi}_k(0, \eta), \ldots, \partial_\eta^s \Lambda_0^r(\eta), \ldots), \tag{179}$$

$$\hat{\mathcal{F}}_1^b(\ldots, \partial_\eta^n A_{kp}(\eta), \ldots, \partial_\eta^n B_{kp}(\eta), \ldots, \partial_\eta^n C_{kq}(\eta), \ldots, \partial_\eta^v \Lambda_1^u(\eta), \ldots)$$

$$= \mathcal{F}_1^b(\ldots, \partial_\sigma^m \partial_\eta^n \hat{\phi}_k(1, \eta), \ldots, \partial_\eta^v \Lambda_1^u(\eta), \ldots), \tag{180}$$

this discretization gives rise to the following system of $NK + 2K + H$ equations

$$\hat{\mathcal{P}}^j_\ell(\ldots, \partial_\eta^n A_{kp}(\eta), \ldots, \partial_\eta^n B_{kp}(\eta), \ldots, \partial_\eta^n C_{kq}(\eta), \ldots) = 0, \tag{181}$$

$$\hat{\mathcal{F}}_1^a(\ldots, \partial_\eta^n A_{kp}(\eta), \ldots, \partial_\eta^n B_{kp}(\eta), \ldots, \partial_\eta^n C_{kq}(\eta), \ldots, \partial_\eta^s \Lambda_0^r(\eta), \ldots) = 0, \tag{182}$$

$$\hat{\mathcal{F}}_0^b(\ldots, \partial_\eta^n A_{kp}(\eta), \ldots, \partial_\eta^n B_{kp}(\eta), \ldots, \partial_\eta^n C_{kq}(\eta), \ldots, \partial_\eta^v \Lambda_1^u(\eta), \ldots) = 0, \tag{183}$$

for the $KN + \sum_{k=1}^{K} Q_k + E_0 + E_1$ functions $\{A_{kp}(\eta), B_{kp}(\eta), C_{kp}(\eta), \Lambda_0^r(\eta), \Lambda_1^u(\eta)\}$. If the powers of the polynomials in (177) are such that

$$\sum_{k=1}^{K} Q_k = 2K + H - E_0 - E_1, \tag{184}$$

then the number of unknown functions balances with the number of equations (181)–(183). In the special (decoupled) case where each ϕ_k appears in only one partial differential equation and is required to satisfy H_k boundary conditions then $H = \Sigma_{k=1}^{K} H_k + E_0 + E_1$. A natural choice for Q_k satisfying (199) in this case is

$$Q_k = H_k + 2. \tag{185}$$

and this is found to be adequate in the general case as well.

Once the basic counting of equations is established the above system can be rewritten in first order form appropriate for numerical integration. This is readily accomplished since the basic equations of the model are quasilinear. The discretisation (189) is designed so that the initial conditions $\{A_{kp}(0), B_{kp}(0), C_{kq}(0)\}$ can be read off from the Fourier transform of the initial data (183). The remaining initial data for the numerical integration is provided by $\{\Lambda_0^r(0), \Lambda_1^u(0)\}$ when required. Taking into account the caveats above the system can be extended to a differential–algebraic system by appending the orthonormality conditions (167).

13. LATERAL WHIRL AND INTERACTION WITH THE BORE-LINER

The mathematical model described in this article can be used in conjunction with various assumptions and approximations. As shown in sections 7–10, when combined with data on frictional interactions and external control torques it yields valuable insights into the inter-relations between torsional and axial vibrations and their effects on the stability of drilling operations. The authors have shown elsewhere that the volatilities suffered by traditional so called "soft-torques" devices* can be understood by taking into account the continuum nature of the drill-string. The model also suggests alternative control strategies ("torsional rectification") that can be fully tested in this context and are shown to be superior for the suppression of torsional "slip–stick" [19]. The model has also been used to gain insight into "snap-buckling" due to non-linear flexural excitations of the drill-string [35]. The interaction of the drill-string with the bore cavity is another potentially hazardous problem for the drilling engineer. Field evidence suggests that if a rotating drill-bit is suddenly arrested (in its translational motion at the rock face) then rapid whirling of the drill-string can occur. The energy transferred to this motion can result in catastrophic collisions of the drill-string with the sides of the bore-hole before rotary control sensors at the top-drive can adjust the drive torque. To explore this phenomenon the model

*Designed to combat the destructive nature of torsional relaxation oscillations.

must be allowed to excite both axial, torsional and lateral degrees of freedom subject to a choice of boundary conditions.

The following six pictures arise as a result of such a simulation in which a drill-bit at the end of a 3000 m drill-string is assumed fixed in its translational motion in contact with the rock surface, while the top-drive is rotating. The drill-string is initially slightly displaced in the **j**-**k** plane as shown in the first picture at time $\eta = 0$ in Figure 9. The other pictures in this figure display the configuration of the drill-string as viewed from the top at subsequent times. When the curve representing the centroid of the drill-string touches the circumference of the shaded circle the physical drill-pipe is then in contact with the steel bore-liner at that point. The sequence indicates that a collision with the bore-liner occurs after about two seconds and another after about six seconds. Figures 10 and 11 display the associated **i** and **j** components of the velocity of the drill-string during this period. The effects of the impact are clearly visible in Figures 12 and 13. These display the reaction experienced by the drill-string at the BHA. At about two and six seconds into the simulation both the **i** and **j** components of this reaction increase in both magnitude and frequency. Such signals should be readily detectable and might be used as input in a suitably designed feedback device that controls fluid pressures in the environment of the drill-string. Figure 14 displays the vertical **k** component of the reaction force on the drill-bit (dynamic "weight-on-bit") relative to the top-tension at the rotary. The full dynamic history of the axial vibration speed in the drill-string is displayed in Figure 15 and is commensurate with the fluctuating "dynamic weight on bit" in the previous figure. It is of interest to note the difference in frequency between the axial and lateral vibration in this phase of the evolution, most of the activity residing in the lateral whirling motion of the drill-string.

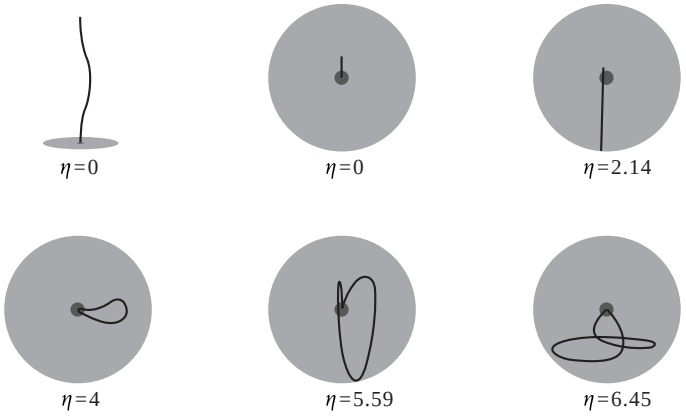

Figure 9. The six pictures in this figure arise from a simulation in which a drill-bit at the end of a 3000 m drill-string is assumed fixed in its translational motion, in contact with the rock surface, while the top-drive is rotating. At time $\eta = 0$ the drill-string is initially slightly displaced in the **j**-**k** plane as shown in the first picture (side view, not to scale, with the drill-bit at the bottom). The other pictures in this figure display the configuration of the drill-string as viewed from the top at subsequent times. When the curve representing the centroid of the drill-string touches the circumference of the shaded circle the physical drill-pipe is then in contact with the steel bore-casing at that point. The sequence shows a whirling drill-string in collision with the bore-casing after about two and then six seconds.

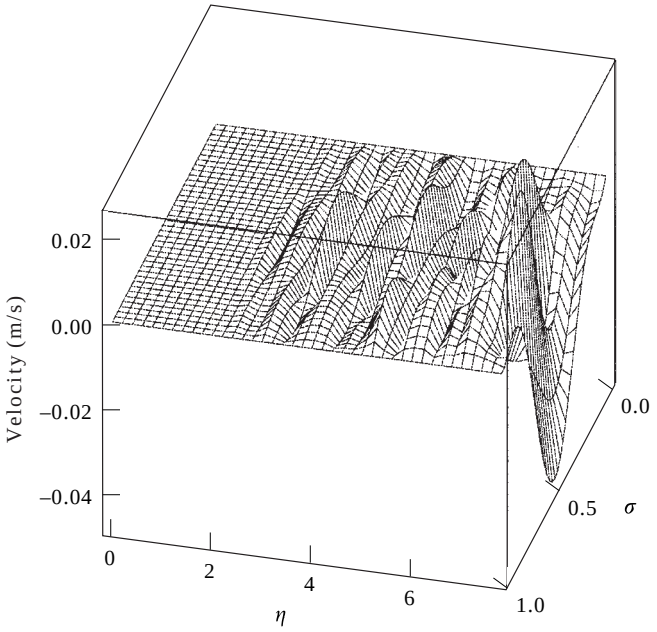

Figure 10. **i** component of the velocity of the drill-string during the period in which the drill-string impacts twice with the bore-liner.

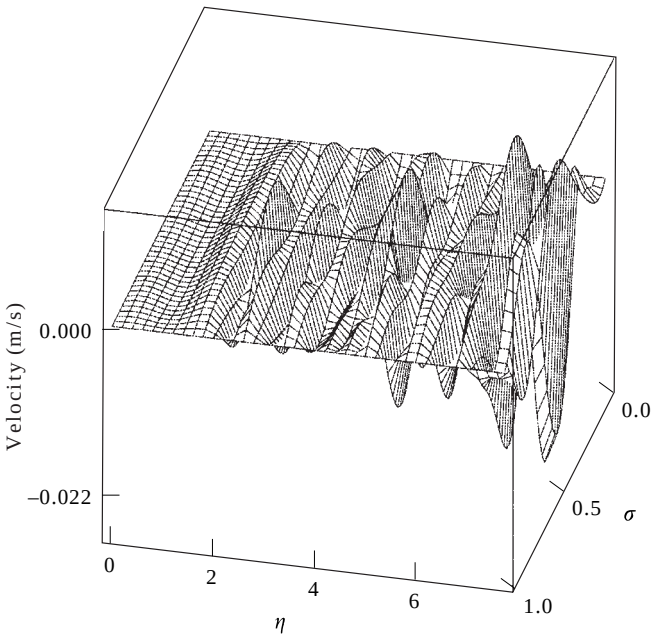

Figure 11. **j** component of the velocity of the drill-string during the period in which the drill-string impacts twice with the bore-liner.

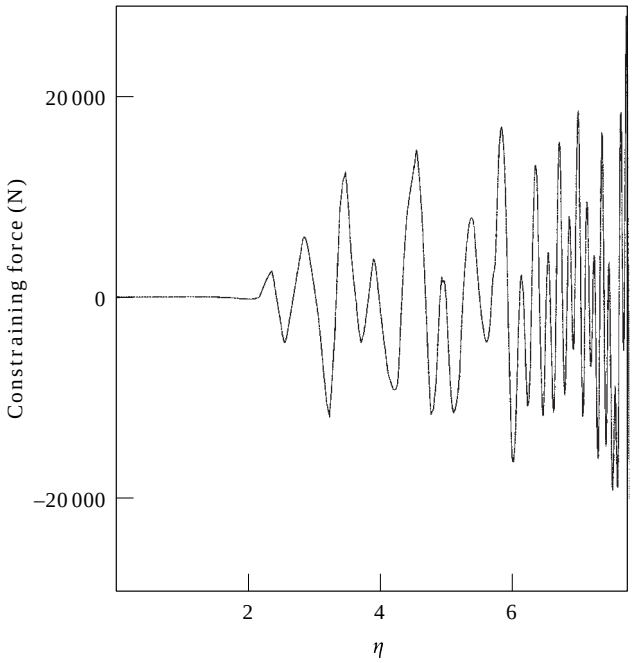

Figure 12. **i** component of the constraining reaction between the drill-string and the BHA during the period in which the drill-string impacts twice with the bore-liner after about $\eta = 2$ and $\eta = 6$ seconds. At each impact there is an increase in the magnitude and frequency of the vibration.

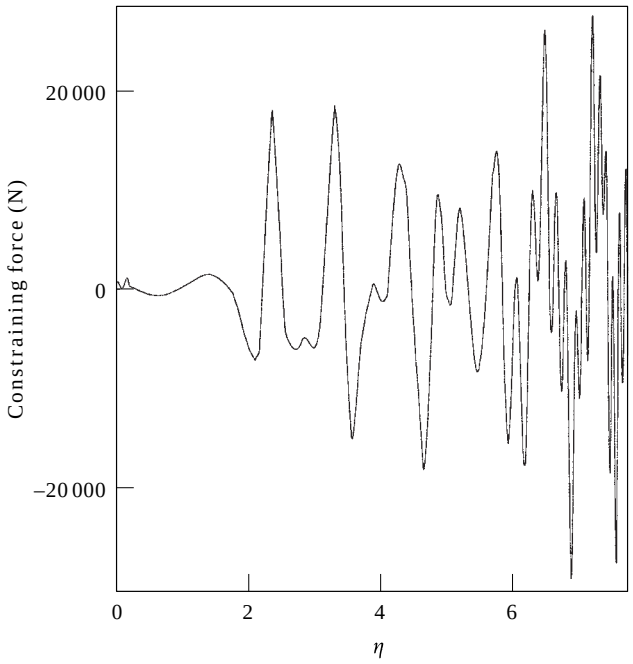

Figure 13. **j** component of the constraining reaction between the drill-string and the BHA during the period in which the drill-string impacts twice with the bore-liner after about $\eta = 2$ and $\eta = 6$ seconds. At each impact there is an increase in the magnitude and frequency of the vibration.

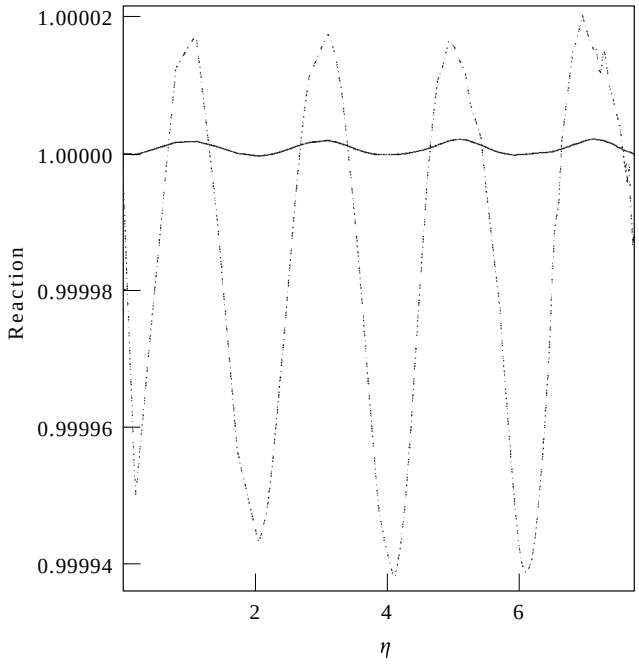

Figure 14. **k** component of the reaction force (· · · · · ·) on the drill-bit ("weight-on-bit") relative to the top-tension at the rotary (—) during the period in which the drill-string impacts twice with the bore-liner after about $\eta = 2$ and $\eta = 6$ seconds. Note the difference in frequency between the axial and lateral vibration in this phase of the evolution.

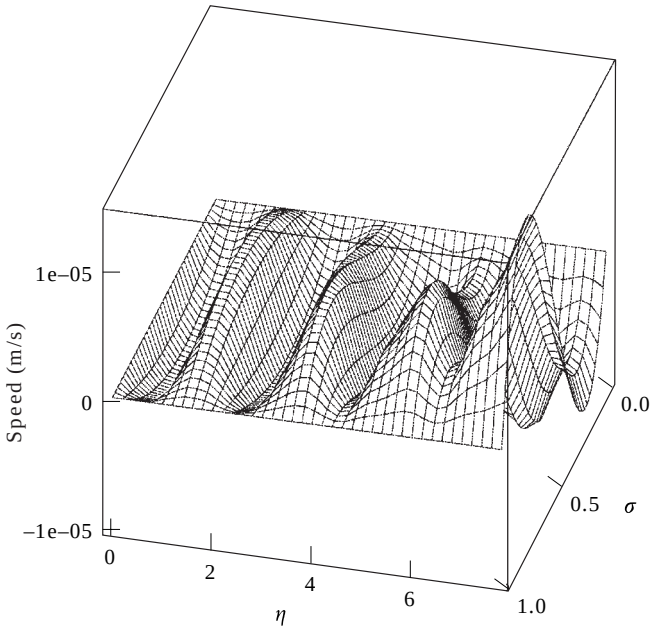

Figure 15. The full dynamic history of the axial vibration speed in the drill-string during the period in which the drill-string impacts twice with the bore-liner.

14. CONCLUSIONS

Some of the dynamical properties of the active components of a drilling assembly have been described above in terms of a simple Cosserat model. It is stressed that all the equations of motion arise from the "geometrically exact" vector equations (1) and (2) together with a prescription of constitutive relations and external forces and torques. Many of the approximations in the literature can be readily derived from such a model. However with a little extra effort the inclusion of axial, lateral and torsional interactions can be fully accommodated with realistic boundary conditions and the domain of validity of numerous approximations deduced more reliably. The model has been used in this paper to discuss the stability of vertical axi-symmetric configurations under both coupled torsional, axial and lateral perturbations. In the axi-symmetric configuration a novel reduction to a system of coupled differential–difference equations is possible. This offers a means of exploring non-perturbative vibrational states with higher resolution than is normally possible by numerical analysis of coupled partial differential equations. Such simulations have demonstrated the limitations inherent in the neglect of axial vibrations in the detection and control of torsional relaxation oscillations. For non-axisymmetric configurations an account has been given of the use of fast Fourier transform techniques in the establishment of a new discretisation approach that may be used to integrate the model under a wide variety of initial conditions. These have included a study of non-perturbative coupled vibrational states under extreme conditions of lateral whirl.

The computations have been coded in MapleV and C^{++} using recently developed techniques of *automatic differentiation* [36]. The former has been used to generate the equations of motion symbolically and display the data graphically while the latter was more efficient for the numerical work. The calculations were performed on an Alpha workstation. The simulations discussed in Section 13 were the most computationally intensive of those presented in this paper. The C^{++} calculations leading to Figures 8–14 took 120 min.

As a result of these computations the authors believe that the integrated model discussed above has a wide domain of applicability. The model can be extended in a number of ways to include more realistic interactions of the drill-string and BHA with their environments. It could also be useful for investigating the vortex induced vibration of marine risers in shear flow that are responsible for instabilities that occur in off-shore drilling operations. It offers practical guides to engineering problems [7, 19, 27, 35] and provides an efficient means of gaining both detailed information and broad insights into the delicate dynamical behaviour associated with "strings" with attachments.

ACKNOWLEDGMENTS

The authors are most grateful to F. Abbassian, S. Antman, M. Fear, B. K. Jones, S. Parfitt and J. Schray for their valuable advice in this investigation and to the Leverhulme Trust, EPSRC and BPX for financial support.

REFERENCES

1. A. Berlioz, J. der Hagopian, R. Dufour and E. Draoui 1996 *ASME Journal of Vibration and Acoustics* **118**, 292–298. Dynamic behaviour of a drill-string: experimental investigation of lateral instabilities.
2. R. F. Mitchell and M. B. Allen 1985 *World Oil* 101–104. Lateral vibration: the key to BHA failure analysis.
3. J. K. Vandiver, J. W. Nicholson and R. J. Shyu 1990 *SPE* **5**, 282–290. Case studies of the bending vibrations and whirling of drill collars.
4. A. P. Christoforou and A. S. Yigit 1997 *Journal of Sound and Vibration* **206**, 243–260. Dynamic modelling of rotating drill-strings with borehole interactions.
5. A. S. Yigit and A. P. Christoforou 1998 *Journal of Sound and Vibration* **215**, 167–181. Coupled torsional and bending vibrations of drill-strings subject to impacts with friction.
6. S. V. Belokobyl'skii and V. K. Prokopov 1982 *Soviet Applied Mechanics* **18**, 1134–1138. Friction-induced self-excited vibrations of drill rig with exponential drag law.
7. G. W. Halsey, A. Kyllingstad and A. Kylling 1988 *Proceedings of the* 63*rd SPE Annual Technical Conference and Exhibition, Houston, Paper* 18049. Torque feedback used to cure slip-stick motion.
8. A. Tondl 1975 *Journal of Sound and Vibration* **42**, 251–260, Quenching of self-excited vibrations: equilibrium aspects.
9. J. D. Janson and L van den Steen 1995 *Journal of Sound and Vibration* **179**, 647–668. Active damping of self-excited torsional vibrations in oil well drill-strings.
10. J. F. Brett 1991 *SPE/IADC Drilling Conference, Amsterdam, paper* 21943. The genesis of bit-induced torsional drill-string vibrations.
11. R. P. Dawson, Y. Q. Lin and P. D. Spanos 1987 *Spring Conference of the Society for Experimental Mechanics, Houston*. Drill-string slip-stick oscillations.
12. P. Sananikone, O. Kamoshima and D. B. White 1992 *Proceedings of the IADC/SPE Drilling Conference, New Orleans, Paper* 23891. A field method for controlling drill-string torsional vibrations.
13. M. P. Dufeyte and H. Henneuse 1991 *SPE/IADC Drilling Conference, Amsterdam, Paper* 21945. Detection and monitoring of the slip-stick motion: field experiments.
14. V. A. Dunayevsky, F. Abbassian and A. Judziz 1993 *SPE Drilling and Completion* 84–92. Dynamic stability of drill-strings under fluctuating weight on bit.
15. M. J. Fear and F. Abbassian 1994 *SPE* 28908, 433–448, Experience in the detection and suppression of torsional vibration from mud logging data.
16. S. Antman 1991 *Non-linear Problems in Elasticity, Applied Mathematical Sciences* 107. N.Y.: Springer-Verlag.
17. T. V. Duggan 1971 *Power Transmission and Vibration Control in Design*. London: ILIFFE.
18. D. J. Struik 1957 *Lectures on Classical Differential Geometry*. Reading, M.A.: Addison-Wesley.
19. R. W. Tucker and C. Wang 1997 *Journal of Sound and Vibration*, (to appear). On the effective control of torsional vibrations in drilling systems.
20. I. L. Singer and H. M. Pollock (editors) 1992 *NATO ASI Series* (220), Kluwer Academic Press. Fundamentals of friction: macroscopic and microscopic processes.
21. M. A. Heckl and I. D. Abrahams 1996 *Journal of Sound and Vibration* **193**, 417–426. Active control of friction-driven oscillations.
22. F. J. Elmer 1997 *Journal of Physics A: Math. Gen.* **30**, 6057–6063, Non-linear dynamics of dry friction
23. S. Cull and R. W. Tucker 1999 *Journal of Physics A (Math. Gen)* **32**, 2103–2113. On the modelling of coulomb friction.

24. J. J. STOKER 1950 *Nonlinear Vibrations in Mechanical and Electrical Systems*. Chichester: J. Wiley.
25. J. SCHRAY and R. W. TUCKER 1995 *Lancaster University Report*. The stability of extended string models.
26. V. A. DUNAYEVSKY and F. ABBASSIAN 1995 *BP technical report, SPE* 30478. Application of stability approach to bit dynamics.
27. R. W. TUCKER and C. WANG 1997 *http://www.lancs.ac.uk/users/SPC/Physics.htm*. The excitation and control of torsional slip–stick in the presence of axial vibrations.
28. R. BELLMAN and K. L. COOKE 1963 *Differential Difference Equations*. London: Academic Press.
29. R. D. DRIVER 1977 *Ordinary and Delay Differential Equations, Applied Mathematical Sciences* **20**. Berlin: Springer Verlag.
30. S. P. TIMOSHENKO and J. E. GERE 1961 *Theory of Elastic Stability*. New York: McGraw-Hill.
31. J. W. S. RAYLEIGH 1945 *The Theory of Sound, Volume* 1. New York: Dover.
32. W. T. THOMAS 1997 *The Theory of Vibrations with Applications*. Chapman and Hall.
33. J. N. ORTEGA and W. G. POOLE Jr. 1981 *An Introduction to Numerical Methods for Difference Equations*. Pitman.
34. K. E. BRENAN, S. L. CAMBELL and L. R. PETZOLD 1996 *Classics in Applied Mathematics* **14**, *SIAM*. Numerical solution of initial-value problems in differential–algebraic equations.
35. R. W. TUCKER, R. S. TUNG and C. WANG 1998 *Non-linear Flexural Excitations and Drill-string Dynamics*. Lancaster University Preprint.
36. A. GRIEWANK, D. JUEDES and J. UTKE 1996 *ACM TOMS* **22**, 131–167. *Algorithm* 755. ADOL-C: A package for the automatic differentiation of algorithms written in C/C++.

APPENDIX 1

A.1.1 CONVERSION OF DIMENSIONLESS VARIABLES TO DIMENSIONED VARIABLES

Acceleration of gravity	$g \mapsto g(\rho_0 L_0/E)$
Body force per unit unstressed length of rod	$\mathbf{f} \mapsto \mathbf{f}\, L_0/(EA)$
Body torque per unit unstressed length of rod	$\mathbf{l} \mapsto \mathbf{l} L_0/\mathcal{G}$
Rod location	$\mathbf{R} \mapsto \mathbf{R}/L_0$
Local director angular velocity	$\mathbf{w} \mapsto \mathbf{w} T_0$
Contact force	$\mathbf{n} \mapsto \mathbf{n}/(EA)$
Natural torque unit	$\mathcal{G} = GK_{\alpha\alpha}/L_0$
Natural reference speed	$C = \sqrt{E/\rho_0}$
Contact torque	$\mathbf{m} \mapsto \mathbf{m}/\mathcal{G}$
Extension and shear strain vector	$\mathbf{v} \mapsto \mathbf{v}$
Flexure and torsional strain vector	$\mathbf{u} \mapsto \mathbf{u} L_0$
Rod rotary inertia tensor per unit reference length	$\rho\mathbf{I} \mapsto \rho\mathbf{I} L_0/(T_0^2\mathcal{G})$
Director components of rod rotary inertia tensor per unit reference length	$\mathbf{I}_{jk} \mapsto \mathbf{I}_{jk} c^2/(GK_{\alpha\alpha})$
End attached rotary inertia tensor	$\mathbf{J}_{ik}^T \mapsto \mathbf{J}_{ik}^T/(T_0^2\mathcal{G})$
End attached mass	$\mu^T \mapsto \mu^T c^2/(EAL_0)$
End external force	$\mathbf{F}_{\text{ext}} \mapsto \mathbf{F}_{\text{ext}}/(EA)$
End external torque	$\mathbf{L}_{\text{ext}} \mapsto \mathbf{L}_{\text{ext}}/\mathcal{G}$

A.1.2 NUMERICAL DATA

Operational tensions in the top cable vary considerably but a typical value is 3000 KN or 675 kip. Average "weight-on-bit" values vary up to 250 kN or 65 kip. The following typical values have been used to generate the dimensionless parameters used in the numerical simulations.

TABLE 1

Variable	Symbol	MKS value	MKS dimension
Mass density	ρ	$8{\cdot}009 \times 10^3$	ML^{-3}
Sectional area	A	$3{\cdot}4 \times 10^{-3}$	L^2
Young's modulus	E	$0{\cdot}207 \times 10^{12}$	$ML^{-1}T^{-2}$
Shear modulus	G	$0{\cdot}796 \times 10^{11}$	$ML^{-1}T^{-2}$
Torsional rigidity	$\mathcal{D}$	$9{\cdot}461 \times 10^5$	ML^3T^{-2}
Reference lengths	L_0	$(3\text{–}6)\ 10^3$	L
Reference torque	$\mathcal{G}$	$2{\cdot}9 \times 10^2$	ML^2T^{-2}
Reference speed	c	$5{\cdot}084 \times 10^3$	LT^{-1}
Reference intervals	T_0	0·6–1·2	T
Axial speed	c_a	$5{\cdot}084 \times 10^3$	LT^{-1}
Torsional speed	c_τ	$3{\cdot}152 \times 10^3$	LT^{-1}
Rotary inertia	I_{11}	$4{\cdot}7 \times 10^{-2}$	ML
Rotary inertia	I_{22}	$4{\cdot}7 \times 10^{-2}$	ML
Rotary inertia	I_{33}	$9{\cdot}5 \times 10^{-2}$	ML
Rotary inertial	J_{33}^T	$5{\cdot}43 \times 10^2$	ML^2
Rotary inertia	J_{33}^B	$4{\cdot}46 \times 10^2$	ML^2
Inertia term	$K_{\alpha\alpha}$	$1{\cdot}19 \times 10^{-5}$	L^4
Effective mass	μ_T	$5{\cdot}08 \times 10^4$	M
Effective mass	μ_B	5×10^3	M
String weights	W	$(0{\cdot}8\text{–}1{\cdot}6) \times 10^7$	MLT^{-2}
Control parameter	κ_p	$7{\cdot}5 \times 10^2$	ML^2T^{-2}
Control parameter	κ_i	51	ML^2T^{-2}

APPENDIX 2

A.2.1 REDUCTION TO COUPLED RETARDED DIFFERENTIAL–DIFFERENCE EQUATIONS

This appendix outlines the method used to reduce the non-linear boundary value problem for a system of linear wave equations in two independent variables to an equivalent system of non-linear retarded functional (differential–difference) equations in one independent variable. This reformulation offers computational advantages in the numerical analysis of such systems.

Suppose $\{\phi_k\}$ $(k = 1, 2, \ldots)$ satisfy on $0 \leqslant \sigma \leqslant 1$ the 2-dimensional wave equations:

$$\ddot{\phi}_k(\sigma, \eta) = \beta_k^2 \phi_k''(\sigma, \eta), \tag{A.2.1}$$

where $\{\beta_k\}$ denote constant wave speeds. The general solutions to (A.2.1) are:

$$\phi_k(\sigma, \eta) = L_k(\sigma + \beta_k \eta) + R_k(\sigma - \beta_k \eta), \tag{A.2.2}$$

for functions $\{L_k, R_k\}$. Differentiating (A.2.2) with respect to η gives

$$\dot{\phi}_k(\sigma, \eta) = \beta_k \dot{L}_k(\sigma + \beta_k \eta) - \beta_k \dot{R}_k(\sigma - \beta_k \eta). \tag{A.2.3}$$

From (A.2.2) the "left-moving wave" $L_k(u)$ and "right-moving wave" $R_k(u)$ are determined up to the addition of constants. Adopting $L_k(0) = R_k(0)$, substituting $\eta = 0$ into (A.2.3) and integrating over σ yields

$$\frac{1}{\beta_k} \int_0^u \dot{\phi}_k(v, 0)\, \mathrm{d}v = L_k(u) - R_k(u). \tag{A.2.4}$$

It follows from (A.2.4) and by substituting $\eta = 0$ into (A.2.2) that $L_k(u)$ and $R_k(u)$ may be expressed as:

$$L_k(u) = \tfrac{1}{2}\phi_k(u, 0) + \frac{1}{2\beta_k} \int_0^u \dot{\phi}_k(v, 0)\, \mathrm{d}v, \tag{A.2.5}$$

$$R_k(u) = \tfrac{1}{2}\phi_k(u, 0) - \frac{1}{2\beta_k} \int_0^u \dot{\phi}_k(v, 0)\, \mathrm{d}v, \tag{A.2.6}$$

in terms of the initial wave configurations $\phi_k(\sigma, 0)$ and the initial time derivatives $\dot{\phi}_k(\sigma, 0)$.

At junctions $\sigma = 0$ and $\sigma = 1$ the waves are subject to sets of dynamic boundary conditions depending on $\phi_k(\sigma, \eta)$ and their partial derivatives evaluated at $\sigma = 0$ and $\sigma = 1$ respectively. In addition a set of "dynamic functions" $\{F_i(\eta)\}$ satisfying a set of prescribed ordinary differential equations may also enter the boundary conditions.

The method of reduction to functional equations will be illustrated for a system of two waves $\{\phi_1(\sigma, \eta), \phi_2(\sigma, \eta)\}$ satisfying wave equations (A.2.1) for $0 \leqslant \sigma \leqslant 1$ and two dynamic functions $\{F_1(\eta), F_2(\eta)\}$ that also couple through the boundary conditions:

$$\dot{\phi}_1(0, \eta) = A_1(\phi_1(0, \eta), \phi_2(0, \eta), F_1(\eta)), \tag{A.2.7}$$

$$\phi_2'(0, \eta) = A_2(\phi_1(0, \eta), \phi_2(0, \eta), F_1(\eta)), \tag{A.2.8}$$

$$\dot{F}_1(\eta) = C_1(\phi_1(0, \eta), \phi_2(0, \eta), F_1(\eta)), \tag{A.2.9}$$

at junction $\sigma = 0$ and

$$\phi_2'(1, \eta) = B_1(\phi_1(1, \eta), \phi_2(1, \eta), F_2(\eta)), \tag{A.2.10}$$

$$\dot{\phi}_2(1, \eta) = B_2(\phi_1(1, \eta), \phi_2(1, \eta), F_2(\eta)), \tag{A.2.11}$$

$$\dot{F}_2(\eta) = C_2(\phi_1(1, \eta), \phi_2(1, \eta), F_2(\eta)), \tag{A.2.12}$$

at junction $\sigma = 1$, for some functions A_1, A_2, B_1, B_2, C_1, C_2.

Inserting (A.2.2) into (A.2.7)–(A.2.12) yields the following functional differential equations:

$$\dot{F}_1(\eta) = C_1(L_1(\beta_1\eta) + R_1(-\beta_1\eta), L_2(\beta_2\eta) + R_2(-\beta_2\eta), F_1(\eta)) \tag{A.2.13}$$

$$\dot{F}_2(\eta) = C_2(L_1(1 + \beta_1\eta) + R_1(1 - \beta_1\eta), L_2(1 + \beta_2\eta) + R_2(1 - \beta_2\eta), F_2(\eta)), \tag{A.2.14}$$

$$\begin{aligned}\beta_1\dot{L}_1(\beta_1\eta) - \beta_1\dot{R}_1(-\beta_1\eta) \\ = A_1(L_1(\beta_1\eta) + R_1(-\beta_1\eta), L_2(\beta_2\eta) + R_2(-\beta_2\eta), F_1(\eta)),\end{aligned} \tag{A.2.15}$$

$$\dot{L}_2(\beta_2\eta) + \dot{R}_2(-\beta_2\eta) = A_2(L_1(\beta_1\eta) + R_1(-\beta_1\eta), L_2(\beta_2\eta) + R_2(-\beta_2\eta), F_1(\eta)), \tag{A.2.16}$$

$$\begin{aligned}\dot{L}_1(1 + \beta_1\eta) + \dot{R}_1(1 - \beta_1\eta) \\ = B_1(L_1(1 + \beta_1\eta) + R_1(1 - \beta_1\eta), L_2(1 + \beta_2\eta) + R_2(1 - \beta_2\eta), F_2(\eta)),\end{aligned} \tag{A.2.17}$$

$$\begin{aligned}\beta_2\dot{L}_2(1 + \beta_2\eta) - \beta_2\dot{R}_2(1 - \beta_2\eta) \\ = B_2(L_1(1 + \beta_1\eta) + R_1(1 - \beta_1\eta), L_2(1 + \beta_2\eta) + R_2(1 - \beta_2\eta), F_2(\eta)).\end{aligned} \tag{A.2.18}$$

The structure of the above equations can be greatly simplified by performing changes of variables according to different ranges of η. To this end introduce, for $i, /, k = 1, /, 2$:

$$\mathcal{F}_{i,1}(\eta) \equiv F_i(\eta), \quad \mathcal{F}_{i,0}(\eta) \equiv F_i(-\eta), \quad \text{for} \quad \eta \geqslant 0 \tag{A.2.19, 20}$$

and

$$\mathcal{L}_{k,1}(\eta) \equiv L_k(\beta_k\eta + 1), \quad \mathcal{L}_{k,0}(\eta) \equiv L_k(-\beta_k\eta), \tag{A.2.21, 22}$$

$$\mathcal{R}_{k,1}(\eta) \equiv R_k(\beta_k\eta + 1), \quad \mathcal{R}_{k,0}(\eta) \equiv R_k(-\beta_k\eta) \tag{A.2.23, 24}$$

for $\eta \geqslant -1/\beta_k$. In terms of these functions the equations (A.2.13–18) together with those obtained by replacing η by $-\eta$ take the following form:

$$\dot{\mathcal{F}}_{1,0}(\eta) = -C_1(\mathcal{L}_{1,0}(\eta) + \mathcal{R}_{1,1}(\eta - 1/\beta_1), \mathcal{L}_{2,0}(\eta) + \mathcal{R}_{2,1}(\eta - 1/\beta_2), \mathcal{F}_{1,0}(\eta)), \tag{A.2.25}$$

$$\dot{\mathcal{F}}_{2,0}(\eta) = -C_2(\mathcal{L}_{1,0}(\eta - 1/\beta_1) + \mathcal{R}_{1,1}(\eta), \mathcal{L}_{2,0}(\eta - 1/\beta_2) + \mathcal{R}_{2,1}(\eta), \mathcal{F}_{2,0}(\eta)), \tag{A.2.26}$$

$$\dot{\mathcal{F}}_{1,1}(\eta) = C_2(\mathcal{L}_{1,1}(\eta - 1/\beta_1) + \mathcal{R}_{1,0}(\eta), \mathcal{L}_{2,1}(\eta - 1/\beta_2) + \mathcal{R}_{2,0}(\eta), \mathcal{F}_{1,1}(\eta)), \tag{A.2.27}$$

$$\dot{\mathcal{F}}_{2,1}(\eta) = C_2(\mathcal{L}_{1,1}(\eta) + \mathcal{R}_{1,0}(\eta - 1/\beta_1), \mathcal{L}_{2,1}(\eta) + \mathcal{R}_{2,0}(\eta - 1/\beta_2), \mathcal{F}_{2,1}(\eta)), \tag{A.2.28}$$

$$\begin{aligned}\dot{\mathcal{L}}_{1,0}(\eta) = &-\dot{\mathcal{R}}_{1,1}(\eta - 1/\beta_1) \\ &- A_1(\mathcal{L}_{1,0}(\eta) + \mathcal{R}_{1,1}(\eta - 1/\beta_1), \mathcal{L}_{2,0}(\eta) + \mathcal{R}_{2,1}(\eta - 1/\beta_2), \mathcal{F}_{1,0}(\eta)),\end{aligned} \tag{A.2.29}$$

$$\begin{aligned}\dot{\mathcal{R}}_{1,0}(\eta) = &-\dot{\mathcal{L}}_{1,1}(\eta - 1/\beta_1) \\ &+ A_1(\mathcal{L}_{1,1}(\eta - 1/\beta_1) + \mathcal{R}_{1,0}(\eta), \mathcal{L}_{2,1}(\eta - 1/\beta_2) + \mathcal{R}_{2,0}(\eta), \mathcal{F}_{1,1}(\eta)),\end{aligned} \tag{A.2.30}$$

$$\begin{aligned}\dot{\mathcal{L}}_{2,0}(\eta) = &\dot{\mathcal{R}}_{2,1}(\eta - 1/\beta_2) \\ &- \beta_2 A_2(\mathcal{L}_{1,0}(\eta) + \mathcal{R}_{1,1}(\eta - 1/\beta_1), \mathcal{L}_{2,0}(\eta) + \mathcal{R}_{2,1}(\eta - 1/\beta_2), \mathcal{F}_{1,0}(\eta)),\end{aligned} \tag{A.2.31}$$

$$\begin{aligned}\dot{\mathcal{R}}_{2,0}(\eta) = &\dot{\mathcal{L}}_{2,1}(\eta - 1/\beta_2) \\ &- \beta_2 A_2(\mathcal{L}_{1,1}(\eta - 1/\beta_1) + \mathcal{R}_{1,0}(\eta), \mathcal{L}_{2,1}(\eta - 1/\beta_2) + \mathcal{R}_{2,0}(\eta), \mathcal{F}_{1,1}(\eta)),\end{aligned} \tag{A.2.32}$$

$$\begin{aligned}\dot{\mathcal{L}}_{1,1}(\eta) = &\dot{\mathcal{R}}_{1,0}(\eta - 1/\beta_1) \\ &+ \beta_1 B_1(\mathcal{L}_{1,1}(\eta) + \mathcal{R}_{1,0}(\eta - 1/\beta_1), \mathcal{L}_{2,1}(\eta) + \mathcal{R}_{2,0}(\eta - 1/\beta_2), \mathcal{F}_{2,1}(\eta)),\end{aligned} \tag{A.2.33}$$

$$\begin{aligned}\dot{\mathcal{R}}_{1,1}(\eta) = &-\dot{\mathcal{L}}_{1,0}(\eta - 1/\beta_1) \\ &+ \beta_1 B_1(\mathcal{L}_{1,0}(\eta - 1/\beta_1) + \mathcal{R}_{1,1}(\eta), \mathcal{L}_{2,0}(\eta - 1/\beta_2) + \mathcal{R}_{2,1}(\eta), \mathcal{F}_{2,0}(\eta)),\end{aligned} \tag{A.2.34}$$

$$\dot{\mathcal{L}}_{2,1}(\eta) = -\dot{\mathcal{R}}_{2,0}(\eta - 1/\beta_2) + B_2(\mathcal{L}_{1,1}(\eta) + \mathcal{R}_{1,0}(\eta - 1/\beta_1), \mathcal{L}_{2,1}(\eta) + \mathcal{R}_{2,0}(\eta - 1/\beta_2), \mathcal{F}_{2,1}(\eta)), \tag{A.2.35}$$

$$\dot{\mathcal{R}}_{2,1}(\eta) = -\dot{\mathcal{L}}_{2,0}(\eta - 1/\beta_2) - B_2(\mathcal{L}_{1,0}(\eta - 1/\beta_1) + \mathcal{R}_{1,1}(\eta), \mathcal{L}_{2,0}(\eta - 1/\beta_2) + \mathcal{R}_{2,1}(\eta), \mathcal{F}_{2,0}(\eta)). \tag{A.2.36}$$

Equations (A.2.25–36) constitute a system of difference–differential equations with retardations $\{1/\beta_k\}$. The required data to integrate this system from $\eta = 0$ to $\eta = \eta_{\max} \geqslant 0$ is $\{\mathcal{F}_{i,0}(0), \mathcal{F}_{i,1}(0)\}$ together with the function values of $\{\mathcal{L}_{k,0}(\eta), \mathcal{R}_{k,0}(\eta), \mathcal{L}_{k,1}(\eta), \mathcal{R}_{k,1}(\eta)\}$ on $-1/\beta_k \leqslant \eta \leqslant 0$.

Indeed using the transformation relations (A.2.19) and (A.2.20) the values of $\{\mathcal{F}_{i,0}(0), \mathcal{F}_{i,1}(0)\}$ can be evaluated from the initial data for $\mathcal{F}_i(\eta)\}$ at $\eta = 0$. Given initial conditions for the waves $\phi_k(\sigma, 0)$ and $\dot{\phi}_k(\sigma, 0)$ on $0 \leqslant \sigma \leqslant 1$ that are consistent with the boundary conditions (A.2.7), (A.2.8), (A.2.9) and (A.2.11), relations (A.2.5) and (A.2.6) can be used to calculate $\{L_k(\sigma), R_k(\sigma)\}$ on $0 \leqslant \sigma \leqslant 1$, which in turn yields the function values of $\{\mathcal{L}_{k,0}(\eta), \mathcal{R}_{k,0}(\eta), \mathcal{L}_{k,1}(\eta), \mathcal{R}_{k,1}(\eta)\}$ on $-1/\beta_k \leqslant \eta \leqslant 0$ by virtue of the transformation relations (A.2.21–24).

To recover the evolution of the waves $\{\phi_1, \phi_2\}$ and the functions $\{F_1, F_2\}$ consider the transformations reciprocal to equations (A.2.19–24). Provided the solutions for $\{\mathcal{F}_{i,0}(\eta), \mathcal{F}_{i,1}(\eta), \mathcal{L}_{k,0}(\eta), \mathcal{R}_{k,0}(\eta), \mathcal{L}_{k,1}(\eta), \mathcal{R}_{k,1}(\eta)\}$ exist in the range $0 \leqslant \eta \leqslant \eta_{\max}$ the functions $\{F_i(\eta)\}$ can be evaluated for $-\eta_{\max} \leqslant \eta \leqslant \eta_{\max}$ according to

$$F_i(\eta) = \mathcal{F}_{i,1}(\eta), \quad \text{for} \quad \eta \geqslant 0 \tag{A.2.37}$$

and

$$F_i(\eta) = \mathcal{F}_{i,0}(-\eta), \tag{A.2.38}$$

for $\eta \leqslant 0$. The left-moving and right-moving waves can also be evaluated as:

$$L_k(\eta) = \mathcal{L}_{k,1}(\eta/\beta_k - 1/\beta_k), \quad R_k(\eta) = \mathcal{R}_{k,1}(\eta/\beta_k - 1/\beta_k) \tag{A.2.39, 40}$$

for $-\beta_k\eta_{\max} \leqslant \eta \leqslant 0$ and

$$L_k(\eta) = \mathcal{L}_{k,0}(-\eta/\beta_k), \quad R_k(\eta) = \mathcal{R}_{k,0}(-\eta/\beta_k), \tag{A.2.41, 42}$$

for $0 \leqslant \eta \leqslant \beta_k\eta_{\max} + 1$. Combining the left-moving and right-moving waves using (A.2.2) then yields the wave functions $\phi_k(\sigma, \eta)$ on $0 \leqslant \sigma \leqslant 1$ and $-\eta_{\max} \leqslant \eta \leqslant \eta_{\max}$.

The boundary problem can therefore be analysed in terms of a system of retarded difference–differential equations. The generalisation to an arbitrary number of waves and dynamic functions follows along similar lines and naturally lends itself to algebraic computation.